AFRL-SR-AR-TR-08-0159

REPORT DOCUMENTATION PAGE

1. REPORT DATE	2. REPORT TYPE	3. DATES COVERED
27-02-2008	Final Report	June 1 to November 30, 2007

4. TITLE AND SUBTITLE

Exploring the Acoustic Nonlinearity for Monitoring Complex Aerospace Structures

5a. CONTRACT NUMBER
FA9550-07-1-0470

5b. GRANT NUMBER

5c. PROGRAM ELEMENT NUMBER

6. AUTHOR(S)

Zagrai, Andrei N. and Doyle, Derek T.

5d. PROJECT NUMBER

5e. TASK NUMBER

5f. WORK UNIT NUMBER

7. PERFORMING ORGANIZATION NAME(S) AND ADDRESS(ES)

New Mexico Institute of
Mining and Technology

801 Leroy Place
Socorro, NM 87801

8. PERFORMING ORGANIZATION REPORT NUMBER

NMT-MENG-2008-LISS-2

9. SPONSORING / MONITORING AGENCY NAME(S) AND ADDRESS(ES)

USAF, AFRL
AFOSR / PKC
875 Randolph St. Room 3112
Arlington, VA 22203

Dr Victor Giurgiutiu/NA

10. SPONSOR/MONITOR'S ACRONYM(S)

11. SPONSOR/MONITOR'S REPORT NUMBER(S)

12. DISTRIBUTION / AVAILABILITY STATEMENT

Approved for public release,
distribution unlimited

13. SUPPLEMENTARY NOTES

14. ABSTRACT

The project explores the acoustic nonlinearity for monitoring complex aerospace structures. A particular attention is given to structural connectors and joints. For these structural elements, an embedded nonlinear ultrasonic (ENU) approach is developed that utilizes unobtrusive piezoelectric wafer active sensors bonded to or embedded into structural elements. The nonlinear manifestation of structural damage is studied and various damage identification methodologies are suggested. Experimental results show feasibility of ENU monitoring of bolted joints in thin-walled aeronautical structures and complex space structures with iso-grinds. The proposed acousto-elastic method has shown potential in quantifying the torque level on a bolt and locating loosened bolts. Promising results were obtained for ENU monitoring of epoxy bonds. Classical and new nonlinear acoustic methods were found to be effective in detecting relatively large damage, but showed misinterpretation errors for specimens with damage of smaller size. A new nonlinear acoustic technique was suggested for short pulse measurements in aerospace structures. Correlation of experimental results obtained with a classical nonlinear acoustic approach and a new technique was established. It is suggested that ENU may be used either as a stand-alone SHM technique or as a complement to existing embedded ultrasonic methods.

15. SUBJECT TERMS

Structural health monitoring, nonlinear elastic waves, embedded ultrasonics, nonlinear diagnostics, aerospace structures, structural joints.

16. SECURITY CLASSIFICATION OF:			17. LIMITATION OF ABSTRACT	18. NUMBER OF PAGES	19a. NAME OF RESPONSIBLE PERSON
a. REPORT	b. ABSTRACT	c. THIS PAGE	SAR	41	Andrei Zagrai
					19b. TELEPHONE NUMBER 575-835-5636

Exploring the Acoustic Nonlinearity for Monitoring Complex Aerospace Structures

Andrei Zagrai* and Derek Doyle†

New Mexico Institute of Mining and Technology,
Department of Mechanical Engineering
801 Leroy Pl., Socorro, NM 87801
575-835-5636, Fax 575-835-5209, azagrai@nmt.edu

REPORT # NMT-MENG-2008-LISS-2

Date: February 27, 2008

* Assistant Professor and PI
† Graduate Student

ABSTRACT

The project explores the acoustic nonlinearity for monitoring complex aerospace structures. A particular attention is given to structural connectors and joints. For these structural elements, an embedded nonlinear ultrasonic (ENU) approach is developed that utilizes unobtrusive piezoelectric wafer active sensors bonded to or embedded into structural elements. The nonlinear manifestation of structural damage is studied and various damage identification methodologies are suggested. Experimental results show feasibility of ENU monitoring of bolted joints in thin-walled aeronautical structures and complex space structures with iso-grinds. The proposed acousto-elastic method has shown potential in quantifying the torque level on a bolt and locating loosened bolts. Promising results were obtained for ENU monitoring of epoxy bonds. Classical and new nonlinear acoustic methods were found to be effective in detecting relatively large damage, but showed misinterpretation errors for specimens with damage of smaller size. A new nonlinear acoustic technique was suggested for short pulse measurements in aerospace structures. Correlation of experimental results obtained with a classical nonlinear acoustic approach and a new technique was established. It is suggested that ENU may be used either as a stand-alone SHM technique or as a complement to existing embedded ultrasonic methods.

Table of Contents

List of Figures

List of Tables

1 INTRODUCTION

1.1 Motivation

Increasing complexity of modern aerospace structures necessitates development of nondestructive evaluation (NDE) and structural health monitoring (SHM) tools integrable into structural fabrication processes and maintenance procedures. Advanced aerospace structures feature structural components with composite cores, ribs, grooves, holes, and various types of joints. Inspection of such structural elements is not trivial and often requires disassembling during assessment or involves use of sophisticated equipment (e.g. CT-Scan) in the off-line mode. Popular SHM methodologies such as vibration monitoring or embedded ultrasonics [1-8] have shown promising results in detection of detrimental conditions in structures of relatively simple geometries (beams, plates, etc.), but revealed limited success in complex media. One perspective approach that may improve performance of the elastic wave propagation SHM methods is embedded nonlinear ultrasonics that explores a nonlinear acoustic manifestation of structural damage as a detection feature. The acoustic nonlinearity is inherent to structural damage and, in contrast to conventional techniques, may allow for discrimination of structural features (holes, grooves) from actual damage because these features do not exhibit the nonlinear response. This result may facilitate damage detection and selectivity in complex structures where misinterpretation is possible if, for example, a technological groove reflects the same amount of the acoustic energy as a propagating crack.

1.2 Practical need

Recent interest in the nonlinear acoustic condition assessment methodology has been in part motivated by its potential in assessing health of structural joints. Practical applications include a variety of adhesive and bolted joints in aeronautical structures and tactical spacecrafts. For instance, there is an urgent need in developing a SHM methodology that would allow for rapid assessment of structural integrity of the Responsive Space satellites. These satellites should be assembled in few days which leaves little time for testing before launch, [9]. Although testing time is limited, for a successive mission it is essential to confirm that (a) structural components have no manufacturing defects and they did not incur any damage during assembly (e.g. a drop of a heavy part on a honeycomb panel), (b) the assembly was done correctly and structural joints and connectors perform adequately. It is critical to ensure that not only each spacecraft component is healthy, but the whole structure will perform adequately during launch. We anticipate that the embedded nonlinear ultrasonics will enable assessment of the joints' integrity and assist in "Go" – "No go" decisions for the tested payload.

1.3 State of the art

Nonlinear ultrasonics has been a successful, but delicate methodology in nondestructive testing. A broad spectrum of research contributions has been focused on connecting characteristics of an incipient material damage and variations of the nonlinear acoustic parameter measured with finite amplitude [10-11], resonance [12-13], and modulation techniques [14-15]. Several studies on the nonlinear acoustic assessment of structural joints have been also reported [16-17]. Although considerable interest in nonlinear ultrasonics is noticeable in the NDE sector, realization of this methodology in the SHM context has been limited [18]. The nonlinear SHM is currently dominated by methodologies exploring structural vibrations at relatively low frequencies [19-21] and hence insensitive to the small-scale local damage. However, it is interesting to note that SHM realization of the embedded nonlinear ultrasonics may exceed potential of the nonlinear ultrasonic NDE methods. A rationale behind this optimistic view is that embedded SHM sensors are fixed and therefore a "sensor baseline" may be effortlessly removed from consideration. This operation would be difficult to achieve with repositionable NDE transducers. In addition, the testing configuration in SHM is fixed and allows for lower variability of measurement values than fast and less repeatable NDE setups. Therefore, we advocate that embedded nonlinear ultrasonics may provide a feasible and effective addition to existing ultrasonic SHM methods. This innovative SHM approach may augment popular embedded ultrasonic and impedance methodologies to yield an additional and "orthogonal" damage signature. However, realization of the embedded nonlinear ultrasonics lacks a basic study on feasibility of the method in the SHM context. The proposed exploratory study is aimed at fulfilling this gap.

2 TECHNICAL OBJECTIVES

The proposed research efforts will be conducted in accordance with the following technical objectives.

1. Investigate feasibility of the embedded nonlinear ultrasonics approach for assessment of structural integrity.
2. Explore damage selectivity of the proposed SHM method.
3. Study nonlinear acoustic manifestation of structural damage in complex aerospace structures.

3 EXPERIMENTAL SAMPLES

Addressing needs of the Responsive Space program for monitoring integrity of satellite components, we focus on the most critical structural elements of the spacecraft: structural panels and joints. Two configurations of experimental samples are considered: 1-D, and realistic satellite panels. The samples includes adhesive and bolted joints.

3.1 1-D specimens

3.1.1 1-D bolted joint specimens

One dimensional specimens were cut from the 2024-T3 aluminum. The following parameters of the alloy were considered: density of 2.78 g/cc, modulus of 72.4GPa, yield of 427MPa, fatigue strength of 124MPa at 5E8 cycles, shear strength of 283MPa and Poisson ratio of 0.33. Each specimen consisted of two aluminum beams (length – 12 in, width – 2 in, and thickness – 0.08 in) connected using a two-bolt joint as depicted in Figure 1. Two 3/8-16 grade 8 hex flange screws having minimum tensile strength of 150 ksi were utilized with accompanying 3/8-16 UNC flange nuts.

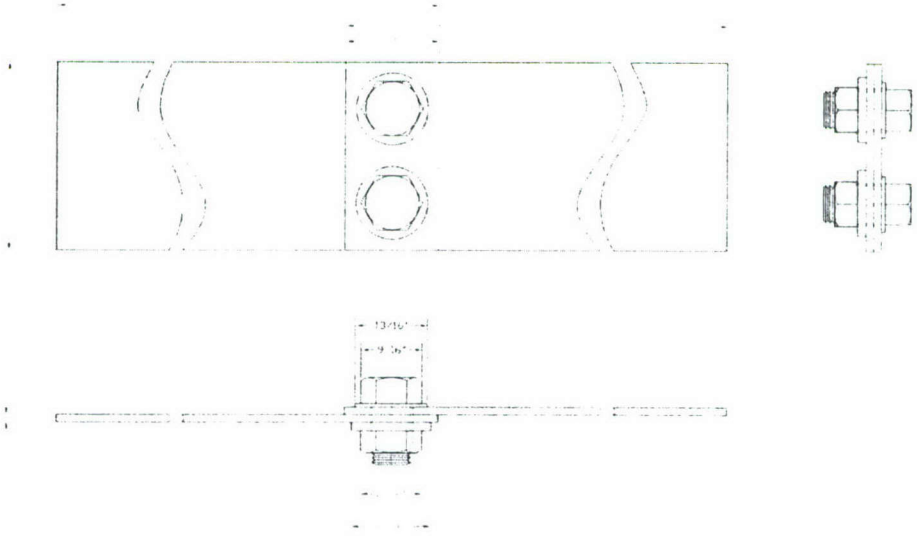

Figure 1 A bolted joint specimen representing 1-D structure.

3.1.2 1-D epoxy bond specimens

The same aluminum alloy (2024-T3) was used to fabricate the epoxy bond specimens. Each experimental specimen consisted of two thin metallic beams bonded with a 3/2 inch overlap. Approximate dimension of the aluminum beams are presented in Figure 2. The epoxy bond was realized with the aerospace grade Hysol® EA 9309NA epoxy. Four configurations of the epoxy bond specimens were considered:

(i) **Ideal bond E0**`: two 12"×2" beams bonded with the 3/2" × 2" inches overlap completely filled with epoxy; i.e. epoxy area $AE_{E0} = 3$ in^2, damaged area $A_{E0} = 0$.

(ii) **Minor disbond E1**`: two10"×2" beams bonded with the 3/2" × 2" inches overlap. A semicircular disbond of $A_{E1} = 0.2$ in^2 was simulated by reducing area covered with epoxy. The remaining area of a bond covered with epoxy is $AE_{E1} = 2.8$ in^2.

(iii) **Medium disbond E2**`: two 12"×2" beams bonded with the 3/2" × 2" inches overlap. A semicircular disbond of $A_{E2} = 0.4$ in^2 was introduced. The remaining area of a bond covered with epoxy is $AE_{E2} = 2.6$ in^2.

(iv) **Large disbond E3`**: two 12"×2" beams bonded with the 3/2" × 2" inches overlap. A rectangular disbond of $A_{E3} = 1$ in^2 was introduced. The remaining area of a bond covered with epoxy is $AE_{E3} = 2$ in^2.

Experimental specimens E0`, E1` and E3` are illustrated in Figure 2. However, practical specimens had two 3/8" holes centered 0.5" from each end and separated by 1".

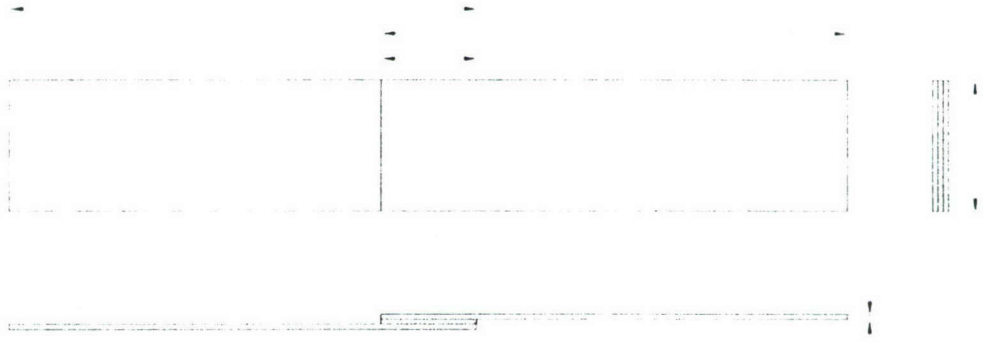

E0`

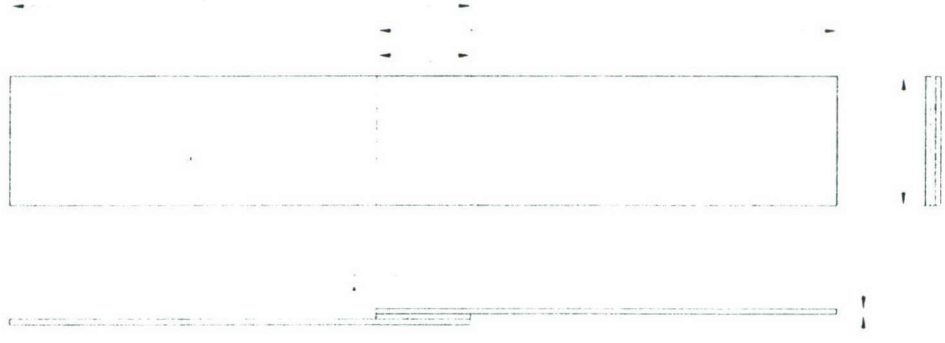

E1`

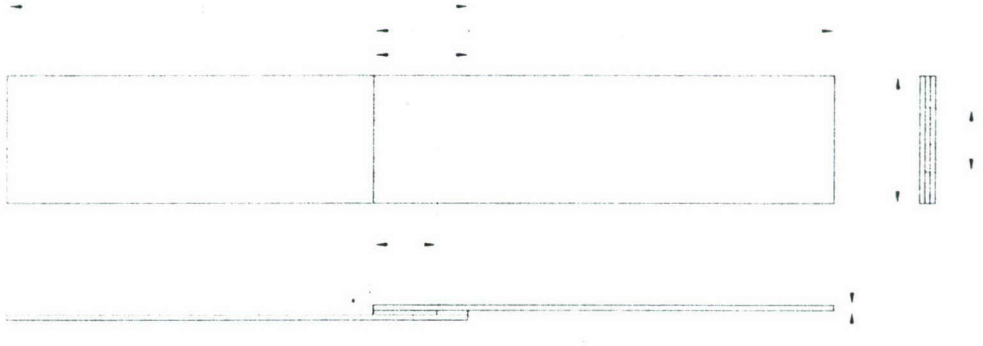

E3`

Figure 2 Epoxy specimens showing an ideal bond E0` and artificially introduced disbonds E1` and E3`.

3.2 Realistic satellite panels

Specification for fabrication of a model of a satellite panel was provided by AFRL SVD Kirtland. The configuration of a panel is depicted in Figure 3.

Four realistic panels were machined from aluminum 6061-T6 plates measuring 18"x18"x0.5". In practical satellite design, two panels connected via bolted and epoxy joints represent one side of the spacecraft. To imitate actual satellite structure, each plate has been machined to establish an iso-grid frame composed of 64-2"x2"x0.75" cutouts with a 0.25" wall thickness. These cutouts are observable in Figure 3 and are used for housing electronic devices and wiring. In the center of each grid junction, a hole was drilled to accommodate a bolt. Each plate contained 49 holes. In the top plate forty nine 0.164" through holes with a 0.27" counter bore 0.164" deep were machined. The bottom plate featured a similar number of threaded holes for #8-32 bolts. Figure 4 illustrates different views of the panel and its plates. The bolts used on the panels were 1" long #8-32 socket cap screws.

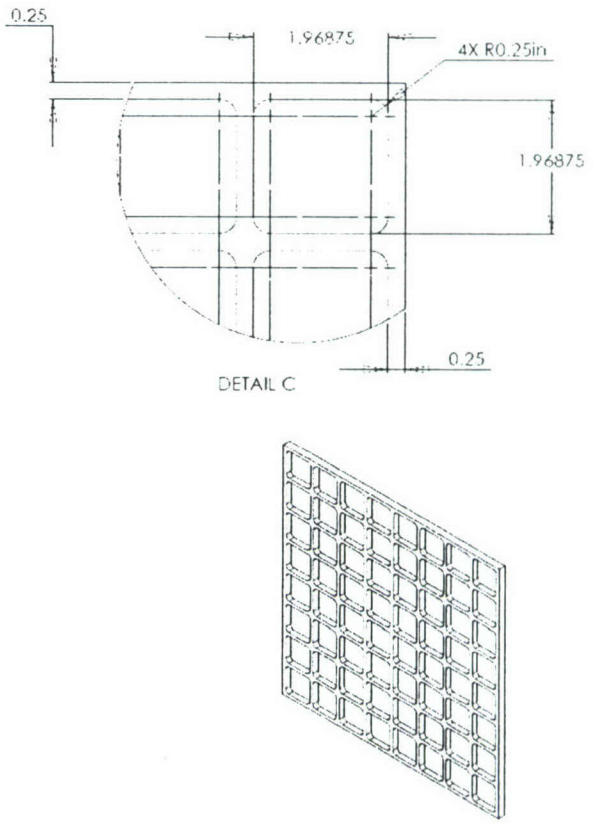

Figure 3 A realistic satellite panel fabricated according to specification provided by Space Vehicles Directorate, Kirtland AFB.

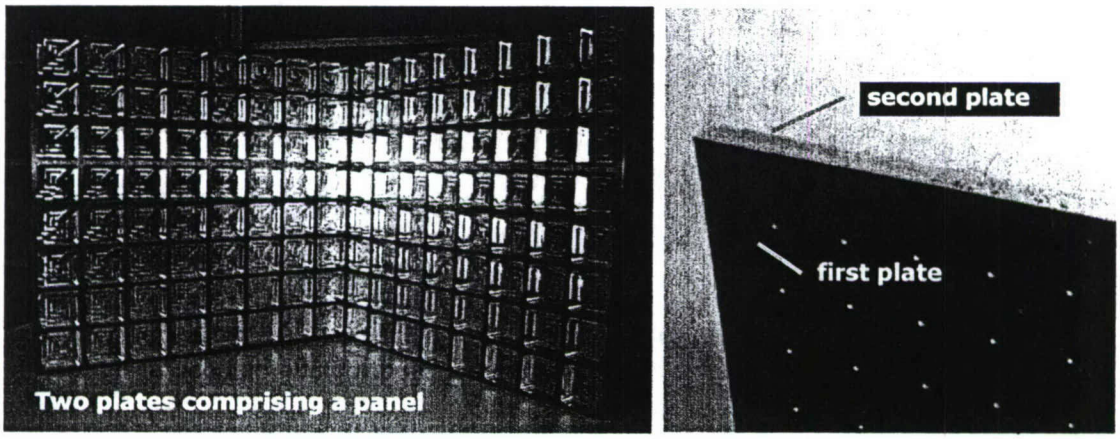

Figure 4 Realistic satellite panel comprised of two aluminum plates with iso-grid frames.

3.3 Honeycomb panel

In addition to panels fabricated from a solid aluminum, we considered a honeycomb aluminum panel. The dimensions of the honeycomb panel designated as specimen HAP1 are as follows: length – 305 mm (12"), width – 305 mm (12"), thickness – 12.7 mm (0.5"). The aluminum alloy used to fabricate the panel was not specified by manufacturer. HAP1 consists of two aluminum sheets of 1 mm thickness bonded with epoxy of unknown origin. Top surfaces of aluminum sheets are painted. The honeycomb section features thin foil (presumably aluminum alloy) with each comb sides of 9.5 mm and 6 mm. A photograph of HAP1 is presented in Figure 5.

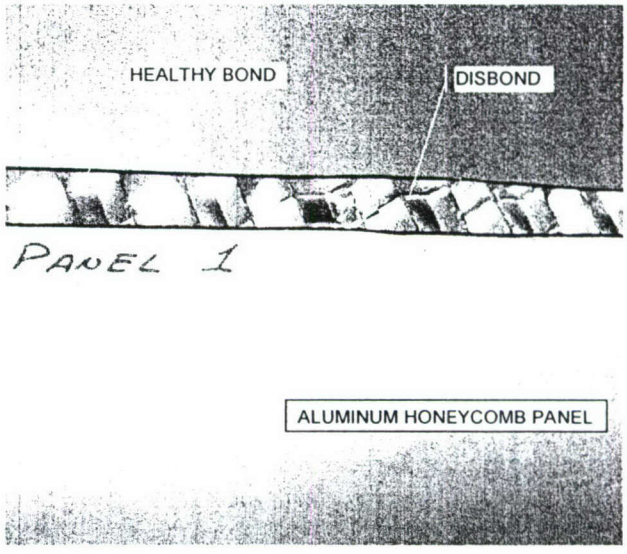

Figure 5 Example of a complex aerospace structure - an aluminum honeycomb panel HAP1.

An artificial disbond was introduced from one side of HAP1 using a spreader bar. Only one (top) aluminum sheet was disbonded from the honeycomb section. Visual inspection of the second (bottom) aluminum sheet did not reveal any damage of the epoxy bond. The edge of a disbond between the top aluminum sheet and the honeycomb structure is noticeable in Figure 5. The actual disbonded area is not known exactly, but it was initiated along a line of 6 cm length.

4 INSTRUMENTATION FOR EMBEDDED NONLINEAR ULTRASONICS (ENU)

4.1 Sensors

Sensing elements employed in this study were fabricated from APC 850 piezoelectric ceramic. Silver electrodes were introduced on the top side of each sensor to facilitate one-side wiring. A typical length of leads was 15 cm. Sensors were installed on a structural surface using a cynoacrylate adhesive. Illustration of a sensor on a specimen with epoxy bond is presented in Figure 6.

Parameters of the sensor and its material characteristics are given in Table 1.

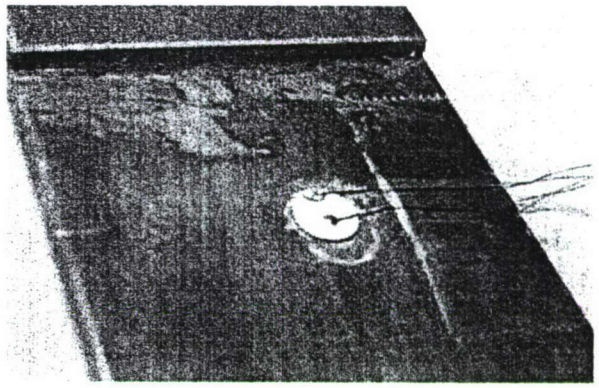

Figure 6 A piezoelectric sensor bonded to aluminum beam

Table 1 Physical dimensions and properties of the APC-850 piezoelectric sensor

Property	Symbol	Value
Radius	r	7 mm
Thickness	h	0.25 mm
Compliance	s_{11}^{E}	$15.300 \cdot 10^{-12}$ Pa^{-1}
Dielectric constant	ε_{33}^{T}	$15.470 \cdot 10^{9}$ F/m
Induced strain coefficient	d_{13}	$-175 \cdot 10^{-12}$ m/V
Coupling factor	κ_{31}	0.360

4.2 Instrumentation

Experimental investigations conducted during the project involved generation and reception of elastic wave in 50 kHz to 1 MHz frequency range. Primary instruments to enable these procedures included Ritec Advanced Measurement (RAM-SNAP 5000) System and NI PXIe chassis with NI 5142 high speed digitizer. At the early stages of the project, Tektronix TDS 2024B digital oscilloscope was used instead of NI PXIe system to collect and analyze experimental data.

A typical experimental setup is depicted in Figure 7. Signal acquisition was synchronized via external triggering from the SNAP system. The Labview® interface of the Tektronix oscilloscope allowed for recording 500 number of points within selected time window. Tektronix 2024B is a 8-bit system with -50 dB noise floor. In general, nonlinear acoustic

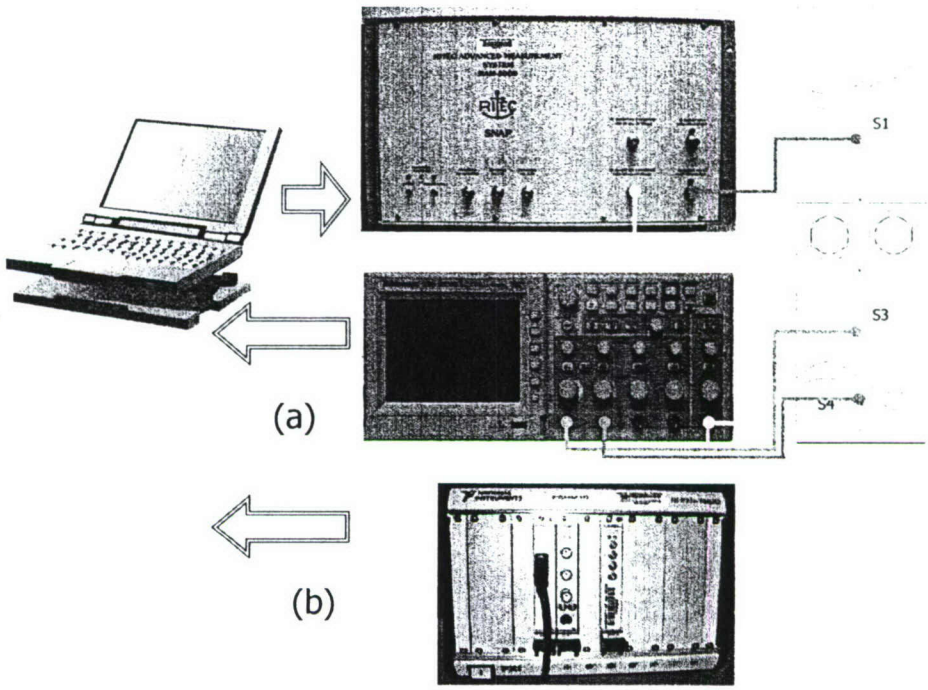

Figure 7 Experimental setup showing connections for SNAP signal generator and Tektronix TDS 2024B Digital Oscilloscope (a). In majority of experiments, a PXI 5142 High Speed Digitizer (b) was used instead of TDS 2024B.

effects are relatively small and are normally manifested at signal levels of approximately -60 dB. For this reason, the 8-bit data acquisition is not the best choice for nonlinear measurements. However, some methodologies, especially those based on a pulse delay, may be adequate provided that the waveform contains enough data points to calculate small phase shifts.

To overcome limitations of the 8-bit system, NI PXI 5142 high speed digitizer (Figure 8) was utilized in majority of tests. The characteristics of a digitizer include 100 MS/s real-time sampling, 2.0 GS/s random-interleaved sampling, 100 MHz bandwidth with noise and anti-aliasing filters, general-purpose alias-protected decimation for all sample rates and quad digital down conversion (DDC) with up to 40 MHz IF bandwidth. Specified resolution of NI PXI 5142 is 14-bits with the noise floor approaching -85 dB. Such a resolution allowed for acquiring at least 10000 data points for a chosen time interval. NI PXI 5142 is a digitizer with two signal channels and a triggering input. The latter was utilized for synchronization with the SNAP system. The setup of a measurement system is presented in Figure 7(b) option. The digitizer was accessed from a PC via a PXI controller integrated in PXIe-1062Q chassis. A Labview® interface was developed for recording time-domain data and calculating parameters of the signal. Spectral analysis was implemented with the same program.

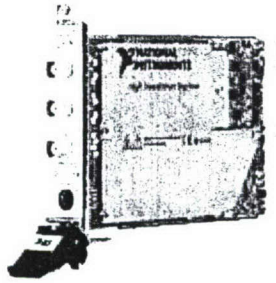

Figure 8 NI PXI 5142 high speed digitizer.

An experimental setup with NI PXI 5142 allowed for substantial improvements in quality of data. This can be inferred from Figure 9 showing comparison of the 8-bit and 14-bit data acquired under identical experimental conditions. To facilitate comparison of the spectral data, we excited a piezoelectric active sensor bonded to aluminum plate with 270 kHz 200 μs pulse. The signal received with a piezoelectric sensor 200 mm away from the excitation point was digitized with TDS 2024B and PXI-5142. Raw data in time and frequency domains are presented in Figure 9. Images of the zoomed-in data give more details on the data quality. In particular, the sample rate of the 8-bit system is very low within the selected window and cannot be used for nonlinear measurements. The 14-bit setup gives an consistent waveform that is noticeably clearer than that of the 8-bit system. The spectrum of the 8-bit signal shows higher noise floor, which precludes observations of spectral components appearing due to nonlinearity. As a result, misinterpretation of data is possible.

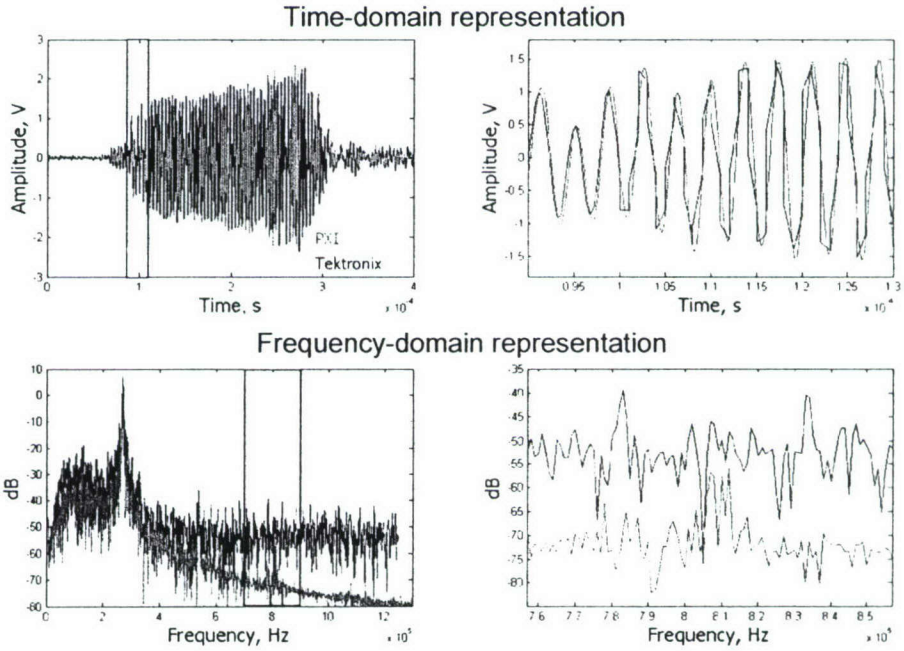

Figure 9 Comparison of the data obtained with 8-bit system (TDS 2024B) – blue and 14-bit system (PXI 5142) – red.

5 ENU SHM OF BOLTED JOINTS

Bolted joints are critical elements of the satellite assembly. One the primary tasks of SHM system for space vehicles is monitoring integrity of bolted joints and quality of epoxy bonds. Following a recommendation of AFRL Space Vehicles Directorate (Kirtland AFB, Albuquerque), our goal was to demonstrate utility of embedded nonlinear ultrasonics in assessing condition of bolted joints connecting typical elements of aeronautical and space vehicles. To achieve this goal, we developed a range of ENU methodologies that can be grouped in short pulse methods and long pulse (quasi-CW) methods.

5.1 Acousto-Elastic Effect in Structural Joints

In developing a methodology for monitoring bolted joints we considered that a bolt exerts a compressive stress on a structural element and therefore sound speed of the elastic wave in a structure will change depending on the value of a torque applied to the bolt. Hence, estimation of the torque can be achieved by measuring delays in propagation of short pulses of elastic waves in structural elements. This approach differs from popular torque measurement techniques based on elastic wave propagation in the bolt itself [22-25].

When the elastic wave travels in the isotropic medium, oscillations in space and time are described by the linear wave equation of the following form.

$$\rho\frac{\partial^2 u_i}{\partial t^2}-\mu\frac{\partial^2 u_i}{\partial x_k^2}-\left(K+\frac{\mu}{3}\right)\frac{\partial^2 u_l}{\partial x_l \partial x_i}=0 \qquad (1)$$

where u_i, u_l are components of a strain tensor $u_{ik}=\frac{1}{2}\left(\frac{\partial u_i}{\partial x_k}+\frac{\partial u_k}{\partial x_i}+\frac{\partial u_l}{\partial x_i}\frac{\partial u_l}{\partial x_k}\right)$, μ is a shear modulus and K is bulk modulus of elastic solid. Equation (1) approximates a generic wave process by neglecting contribution of nonlinear effects.

In practice, the majority of media exhibit a certain degree of nonlinearity with small deviations of the wavefront from idealistic sinusoidal form. Depending on wave propagation conditions, these deviations may accumulate in space and time resulting in a saw tooth or other nonlinear waves [26]. Expansion of the strain energy for small strains [27] leads to nonlinear wave equation, where nonlinear effects are incorporated in the volumetric force term F_i.

$$\rho\frac{\partial^2 u_i}{\partial t^2}-\mu\frac{\partial^2 u_i}{\partial x_k^2}-\left(K+\frac{\mu}{3}\right)\frac{\partial^2 u_l}{\partial x_l \partial x_i}=F_i \qquad (2)$$

$$F_i = \left(\mu + \frac{A}{4}\right)\left(\frac{\partial^2 u_l}{\partial x_k^2}\frac{\partial u_l}{\partial x_i} + \frac{\partial^2 u_l}{\partial x_k^2}\frac{\partial u_i}{\partial x_l} + 2\frac{\partial^2 u_i}{\partial x_l \partial x_k}\frac{\partial u_l}{\partial x_k}\right) +$$
$$+\left(K + \frac{\mu}{3} + \frac{A}{4} + B\right)\left(\frac{\partial^2 u_l}{\partial x_i \partial x_k}\frac{\partial u_l}{\partial x_k} + \frac{\partial^2 u_k}{\partial x_l \partial x_k}\frac{\partial u_i}{\partial x_l}\right) +$$
$$+\left(K - \frac{2\cdot\mu}{3} + B\right)\frac{\partial^2 u_i}{\partial x_k^2}\frac{\partial u_l}{\partial x_l} + \left(\frac{A}{4} + B\right)\left(\frac{\partial^2 u_k}{\partial x_l \partial x_k}\frac{\partial u_l}{\partial x_i} + \frac{\partial^2 u_l}{\partial x_i \partial x_k}\frac{\partial u_k}{\partial x_l}\right) + \cdot$$
$$+(B + 2C)\frac{\partial^2 u_k}{\partial x_i \partial x_k}\frac{\partial u_l}{\partial x_l} \qquad (3)$$

and

Nonlinear wave equation in solids incorporates third-order parameters A, B, and C. Measurement of the indicated nonlinear parameters is a challenging task, which is typically accomplished by means of acousto-elastic method [28]. In the acousto-elastic method, an elastic wave is measured at various static stress levels. Hydrostatic pressurization allows only for determining a combination of third-order moduli. A full set of third-order nonlinear parameters can be obtained through additional uniaxial stress experiments. Previous studies [29] treated a wave propagation medium as infinite solid and presented expressions for a sound speed as a function of applied stress and polarization. It can be shown that accounting for a static uniaxial stress in Equation (3) yields the following identities for sound speeds.

$$\rho c_{l\parallel}^2 = \left(K + \frac{4\mu}{3}\right) - \frac{\sigma}{3K}\left(K - \frac{2\mu}{3} + \frac{K + \mu/3}{\mu}\cdot\left(4K + \frac{22\mu}{3}\right) + \frac{2(K + \mu/3)}{\mu}\cdot A + \frac{4K + 10\mu/3}{\mu}\cdot B + 2C\right) \qquad (4)$$

$$\rho c_{l\perp}^2 = \left(K + \frac{4\mu}{3}\right) + \frac{\sigma}{3K}\left(4K - \frac{8\mu}{3} + \frac{2(K - 2\mu/3)^2}{\mu} + \frac{K - 2\mu/3}{\mu}\cdot A + \frac{2(K + 5\mu/3)}{\mu}\cdot B - 2C\right). \qquad (5)$$

Consider a bolted joint depicted in Figure 10. A quasi-longitudinal wave propagates in plates connected via a bolted joint. Although an elastic wave is not strictly longitudinal, as it is a guided S_0 mode, at low frequencies (lower kHz range) dispersion may be neglected and the expression for a longitudinal wave in infinite medium is suggested for rough estimation of the effect of stress exerted by the joint.

According to Equations (4) and (5) for a uniaxial stress, two orientations with respect to direction of longitudinal wave propagation are possible: (a) applied stress is parallel to displacement in the longitudinal wave – Equation (4) and (b) applied stress is perpendicular to displacement in the longitudinal wave – Equation (5). The bolted joint geometry depicted in Figure 10 implies that material is subjected to the compressive stress perpendicular to direction of the wave propagation. Hence, Equation (5) will be used for estimation of the sound speed changes due to various static loads. It needs to be mentioned that in both equations a compressive stress σ is considered.

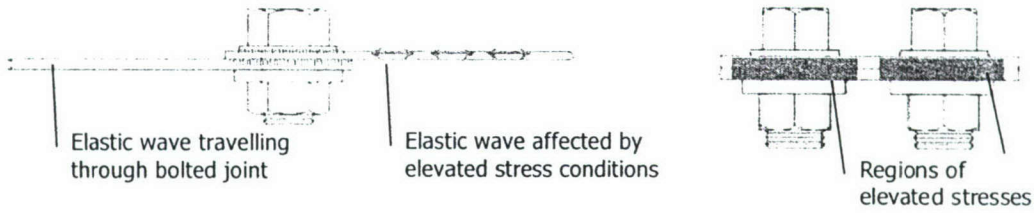

Figure 10 Bolted joint geometry.

From Equation (5) it is apparent that compressive stress σ needs to be estimated first. This can be achieved by considering a force acting on a joint and the effective area over which the applied force is distributed. An equivalent force applied to a single-bolt joint depends on a torque T, bolt diameter d, and torque coefficient k_T.

$$F_T = \frac{T}{k_T \cdot d} \tag{6}$$

Coefficient k_T can be calculated from the joint geometry or found in handbooks on the bolted joints analysis; we will use $k_T = 0.2$ suggested for estimations by Budynas and Nisbett [30]. Given a bolt diameter $d = 9.525$ mm (3/8 in) and a range of torques from 0 to 70 N·m (from 0 to 50 lbs-ft) we arrive to approximate value of 35586 N for the maximum equivalent force. The area of a joint containing most of the stress can be determined from a pressure-cone method

$$A_b = \pi\left(\left(h\tan(\alpha) + \frac{D}{2}\right)^2 - \left(\frac{d}{2}\right)^2\right) \tag{7}$$

where D is the diameter of the washer face and h is the thickness coordinate. For a fixed cone angle $\alpha = 30^\circ$, we estimated $A_b = 343$ mm^2. The compressive stress in the joint is calculated as a ratio of F_T and A_b. A maximum stress is approximately 100 MPa.

Expression (5) features two second-order elastic moduli (K and μ) and three third-order nonlinear coefficients A, B, and C. While the second-order constants are widely available for practically all materials, the third-order constants are reported in limited numbers of studies. For estimation purposes, we utilized data presented by Nagy [31] for aluminum 7064. The numerical values for elastic moduli were calculated from Lame constants and Murnaghan coefficients as follows: $K = 77.56$ GPa, $\mu = 27.4$ GPa, $A = -403$ GPa, $B = -195.5$ GPa, $C = -128.5$ GPa, density $\rho = 2770$ kg/m^3. Substitution in Equation (5) yields sound speeds ranging from 6418 m/s (no stress) to 6411 m/s (for maximum stress of 100 MPa).

5.2 Short Pulse Acousto-Elastic Method

A theoretical explanation presented above suggests that change of the sound speed will lead to a delay in the arriving elastic wave. Therefore, a methodology for assessing torque levels applied to bolts can be realized based on measurements of delay in the time of arrival. This idea can be implemented by transmitting bursts of elastic waves and measuring variation of the propagation time due to torque applied to the bolted joint.

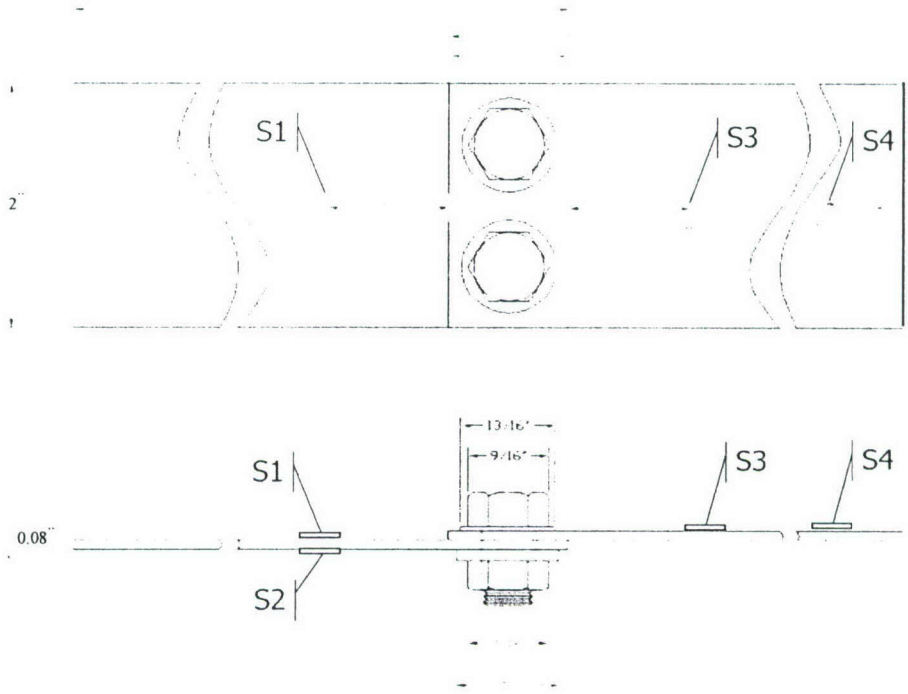

Figure 11 Schematic of bolted joint with indicated sensor locations: S1 S3 and S4 – top surface; S2 – bottom surface.

To validate feasibility of the proposed acousto-elastic method, we conducted a series of tests with a bolted joint specimen depicted in Figure 11. A specimen consisted of two aluminum 2024 beams (length – 12 in, width – 2 in, and thickness – 0.08 in) connected using two 3/8-16, grade 8, hex flange, 1 inch steel screws with accompanying 3/8-16 UNC flange nuts. Holes of 3/8" diameter were drilled approximately 0.5 in from the end of each beam to accommodate screws. Piezoelectric active sensors were fabricated from APC 850 piezoelectric ceramic of the following dimensions: diameter 7 mm, thickness 0.25 mm. Access to the sensor's electrodes was configured from one side (top) via extending a portion of the bottom electrode across sensor's thickness. Active sensors were bonded using a cyanoacrylate adhesive. Position of sensor on a specimen and respective distances to the bolted joints are indicated in Figure 11.

Piezoelectric active sensors were excited with a 3 count 270 kHz pulse provided by the SNAP system. 270 kHz was experimentally determined as a preferable frequency for excitation of S_0 guided mode. This mode was selected due to low dispersion. Experimental setup for this test is depicted in Figure 7. We collected 8-bit and 14-bit data with both sets rendering similar results.

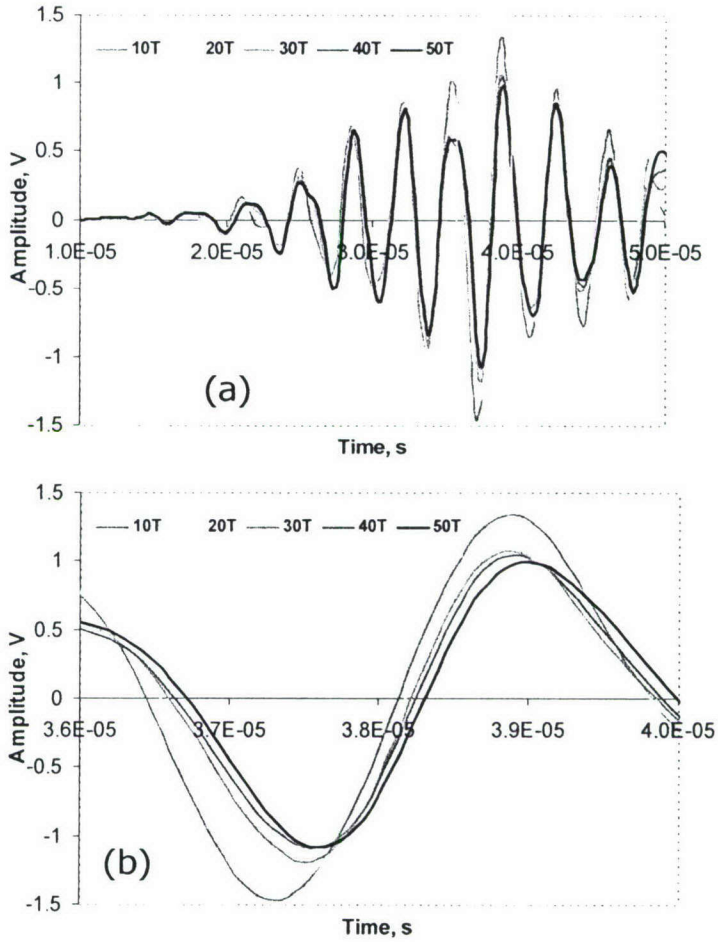

Figure 12 Elastic wave signals recorded at different levels of the applied torque: (a) full record (b) zoomed-in segment.

Tests were conducted according to the following procedure: a 10 ft-lbs torque was applied to both bolts in the joint using an adjustable torque wrench, the specimen was placed on foam and an input signal was supplied to sensor S1, the elastic wave travelled through the joint and was measured with sensor S3. The same procedure was repeated for torque increments of 10 ft-lbs until 50 ft-lbs was reached. This resulted in 5 data records for 10, 20, 30, 40 and 50 ft-lbs respectively. An example of a data set for five levels of torque is depicted in Figure 12. After a waveform at 50 ft-lbs was recorded, the bolts were loosened to relieve stress in the joint and the process was repeated 8 times. As a result, we obtained 8 records for each stress condition (40 records total). The motivation behind this extensive series of tests was to infer statistical properties of data and estimate repeatability.

Our experiments show that torque applied to bolts has a considerable effect on time of arrival and shape of the elastic wave propagated through the joint. Noticeable in the time response depicted in Figure 12, the signal shifts to the right with increased strain in the joint. Figure 12(a) shows a full record of the first pulse arrived at sensor S3. We focused on a first pulse of the S_0 mode because elastic waves arrived later in time consist of a complex

combination of reflected S_0 pulses and diminished contributions of A_0 modes. Although differences between waveforms at increasing torque levels are apparent from Figure 12(a), a detailed picture of the phenomenon can be seen by zooming into a segment of the wave data. As a result, Figure 12(b) shows two important points: (a) increasing of the torque causes pulse delay proportional to the torque level; (b) in additional to changes in temporal characteristics of the signal, changes in the waveform's shape are noticeable at increasing torques.

Table 2 Statistical characteristics of experimental data measured for five values of torque.

Torque, ft*lbs	10	20	30	40	50
Mean Arrival Time, s	2.56684E-05	2.58551E-05	2.58968E-05	2.59834E-05	2.60834E-05
Standard deviation, s	1.59779E-07	9.66223E-08	4.9163E-08	6.05183E-08	3.97702E-08
R^2	0.8298	0.8879	0.9569	0.9603	0.9634

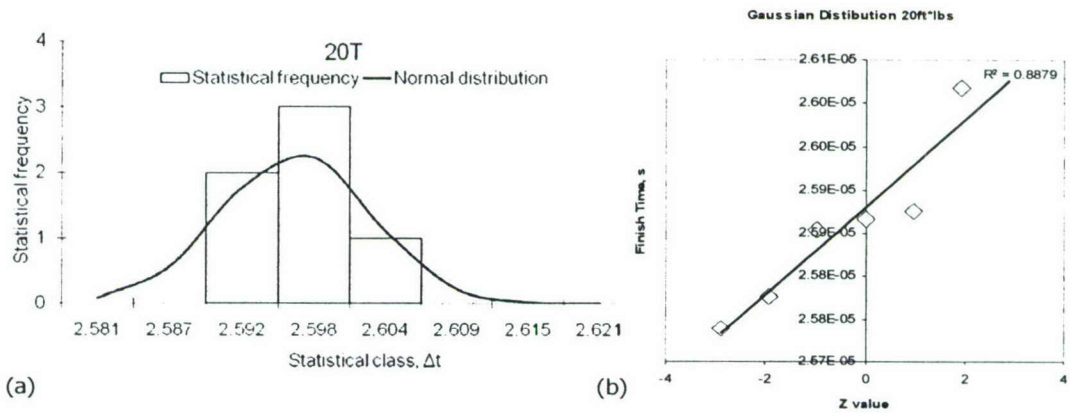

Figure 13 (a) A plot indicating statistical distribution of experimental data for 20 ft-lbs torque and calculated Gaussian distribution; (b) Ordered observations of the pulse arrival times plotted versus standardized Z-scores.

To establish a relationship between torques applied to bolts and respective delays of the signal arrival times, we considered eight measurements for each level of torque. In this study, we did not test for 0 ft-lbs because of difficulties associated with adequate experimental implementation of such a torque. Alternatively, it was decided to interpolate the "0" torque from data for incrementally increased torques. For five levels of torque considered in experiments, a mean value and a standard deviation of the pulse arrival time were calculated for eight trials. More details on statistical analysis of the data is available in Appendix A. Table 2 summarizes statistical properties of data in the acousto-elastic pulse propagation experiment. Statistical distribution of experimental data is important for many aspects of analysis. For this reason, data was grouped in statistical classes according to arrival times and a frequency of occurrence was determined for each class. An example of a plot showing a distribution of experimental data and a fit of a Normal Distribution curve is depicted in Figure 13(a). Assumption of a Normal Distribution was tested by plotting ordered observations of the pulse arrival times versus standardized Z-scores and fitting the resultant data points with a straight line. Figure 13(b) provides an illustration of this

procedure and the R^2 value obtained for the case of 20 ft-lbs. R^2 values close to 1indicate a Normal Distribution of the test data. Results in Table 2 suggest that a Normal statistical distribution may be assumed for practically all torques. However, the case of 10 ft-lbs needs special attention as it shows a broader variability of data. Based on experimental observations and results of statistical analysis Figure 14 was developed, incorporating five data points associated with average values for relative pulse delays and error bars indicating standard deviation margins. According to Figure 14, increase of torque on bolts causes proportional increase in delay of the elastic wave propagating through a joint. Therefore, the proposed method based on nonlinear acousto-elastic effect can be used to quantify the applied torque. Relatively small deviations at high stress levels enable clear separation of torque value. This advantage diminishes at low torques where a broader deviation of experimental data is noticeable. A binary detection (torque vs. no torque) is achievable for practically whole range of torques. Therefore, we conclude that the acousto-elastic method based on nonlinear guided wave propagation has demonstrated considerable potential for assessment of the integrity of bolted joints.

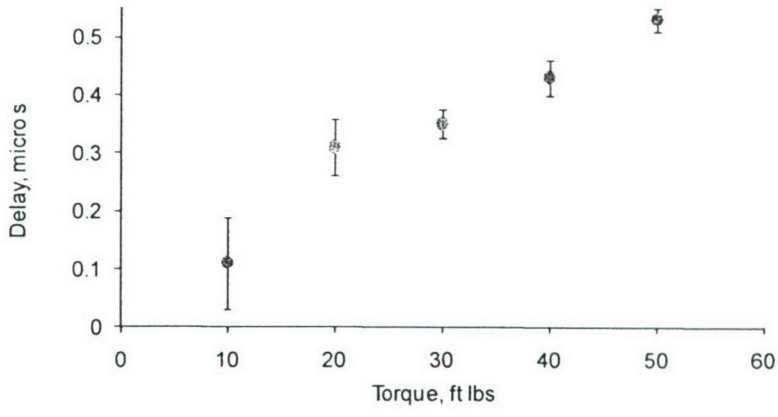

Figure 14 Relative delay of the elastic wave pulse versus applied torque.

5.3 Comparison of Experimental and Theoretical Results

In one of preceding sections we presented a theoretical approach for estimation of effect of stress on the propagating elastic wave. According to development in this section, a maximum stress applied to joint was estimated at 100 MPa. Equation (5) predicts sound speed of 6411 m/s for this value of stress. Delays in pulse arrivals were calculated by considering distance between sensors and size of the stressed region in a specimen. The latter one is difficult to determine without a proper imaging technique. However, it is apparent that the region extends beyond areas under bolts in both width and length directions. Because of the two-dimensional nature of the stress region, we estimated the wave propagation path affected by stress a little over 2 inches. The estimated delays in arrival of the elastic wave under five values of torque are presented in Figure 15 along with experimentally obtained data. As it can be seen from the figure, theory gives

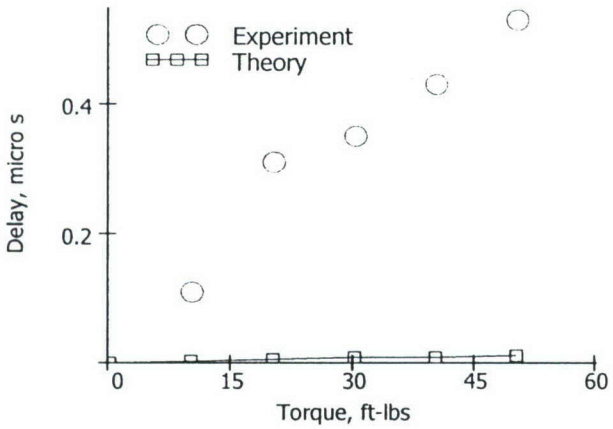

Figure 15 Experimental (red) and theoretical (blue) relative delays in arrival of elastic wave for five values of torque.

approximately an order of magnitude underestimation for pulse delays. This is not surprising as the actual area subjected to stress cannot be determined precisely, nonlinear parameters for aluminum 2024 may differ from 7064 alloy, and most importantly, Equation (5) describes longitudinal sound speed in infinite medium, which differs from the sound speed of quasi-longitudinal plate mode. In fact, this sound speed is lower than in infinite medium and therefore a pulse signal propagating in a plate should show more pronounced changes due to applied static stress.

5.4 Long Pulse Modulation Experiment

In addition to studies involving monitoring of structural integrity using short pulses of elastic waves, we considered employing relatively long pulse signals. Long waveforms are essential for effective implementation of spectral analysis and utilizing spectral features for damage detection.

Long pulses with fundamental frequencies of 270 kHz and 370 kHz were used. Length of both pulses was set to 200 μs bursts. One of these long signals was applied to sensor S1 (see Figure 11 for details) and another one to sensor S2. Hence, location of the excitation was the same, but different sensors were used. Such an experimental configuration allowed for monitoring amplitude levels of higher harmonics and modulation frequencies (e.g. f_1+f_2). In contrast to signal nonlinearity manifesting at higher harmonics (which if often associated with test equipment), modulation components appear only due to nonlinear interaction within experimental samples and may provide information on physical nonlinearity [18]. The transmitted signal was received with a sensor located close to the joint (S3) and a sensor positioned approximately 9.5 inches away from the joint (S4). Two levels of torque were considered in this study: 10 ft-lbs (marked "Loose") and 50 ft-lbs (marked "Tight"). Figure 16 shows frequency spectra obtained at S3 and S4 locations for tight and loose conditions. Several observations can be inferred from Figure 16. In general, amplitude of spectral components in the tight condition is higher than in loose condition. For example, amplitude of a fundamental frequency of 370 kHz in S3 increased 10 dB after bolts were tightened. Such a behavior of fundamental components may be explained by reduced loses of the wave energy in the tight joint [23]. Figure 16b however indicates that although the difference diminishes further away from the joint, most of additional spectral components associated with nonlinear behavior shows higher amplitudes in tight condition. Noticeably, stress exerted by bolts affects amplitude

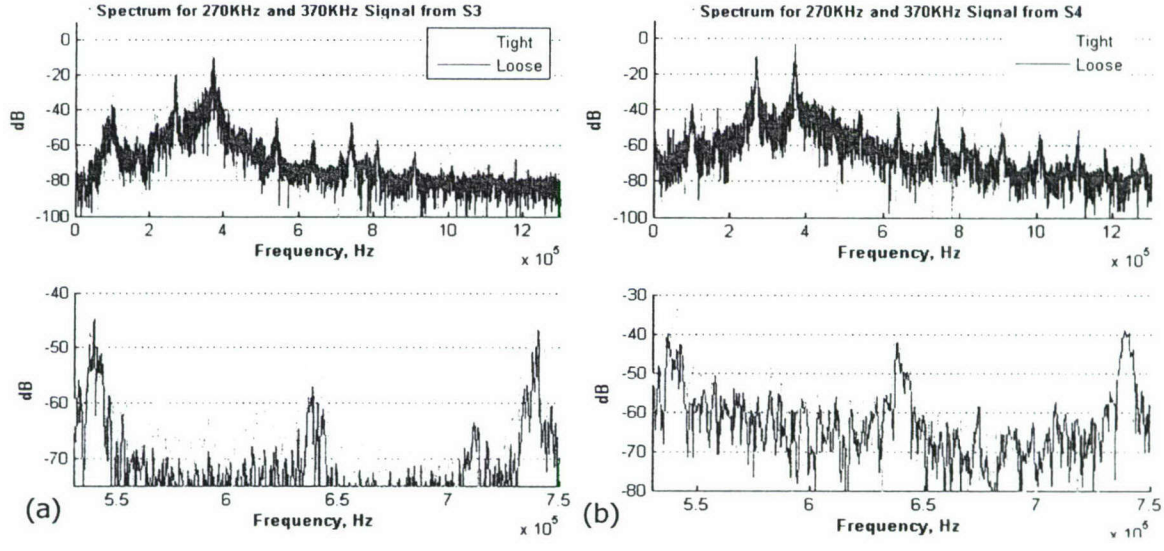

Figure 16 Frequency spectrum (dB re 1V) measured in "tight" and "loose" conditions at locations S3 (a) and S4 (b).

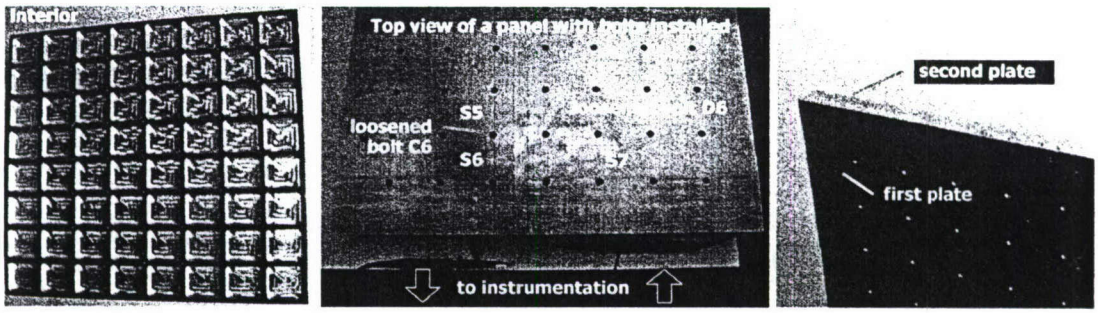

Figure 17 Realistic satellite panel comprised of two aluminum plates with iso-grid frames.

of harmonics and modulation frequencies, but using this feature for quantifying torques requires some serious considerations.

In the presented variant of the modulation technique, long pulse signals were used (some researchers employed CW excitation [32]). This type of excitation results in a standing wave pattern rather than in a propagating elastic disturbance, which leads to high amplitudes at resonance frequencies and very small amplitudes at anti-resonance frequencies. Since without prior measurement of the frequency response, location of maximums and minimums is unknown, misinterpretations are possible in quantifying amplitudes of frequency components in the spectrum. For successful realization of a long pulse or CW methods either additional measurement of the frequency response is needed or implementation of an averaging procedure similar to one suggested by Donskoy *et al.* [14] is required.

5.5 ENU Monitoring of a Realistic Satellite Panel

A short pulse acousto-elastic technique described earlier in this report was validated on a realistic structural specimen representing an actual satellite panel. The panel was fabricated from two aluminum 6061-T6 plates measuring 18"x18"x0.5". To imitate a typical spacecraft design and reduce weight, each plate has been machined to establish an iso-grid frame composed of 64-2"x2"x0.75" cutouts with a 0.25" wall thickness. In the center of each grid junction, a hole was drilled to accommodate a bolt. Each plate contained 49 holes. In the top plate 49 0.164" through holes with a 0.27" counter bore 0.164" deep were machined. The bottom plate featured a similar number of threaded holes for #8-32 bolts. Figure 17 illustrates different views of the panel and its plates. The bolts used on the panels were 1" long #8-32 socket cap screws. To facilitate referencing, the panel was labeled with a grid layout of A-G x 1-7. In the acousto-elastic experiment, piezoelectric active sensors were installed on a surface of the satellite panel between columns C and E and rows 5 and 7. Distance between sensors was set to 2 inches. Figure 17 gives detailed location of sensors. Initially, one sensor (S7) was connected to SNAP signal generation unit, while the other sensor (S6) acted as a receiver. In the first step of the experiment, all 49 bolts were tightened with a 9/64" hex key. The signal utilized in this test was three count 270 KHz pulse. Illustration of the signal transmitted by S7 across the plate is presented in Figure 18. The elastic wave was measured with S6. The received signal was then fed to the NI PXI 5142 card, digitized and recorder for future reference. The record of the elastic wave signal corresponding to a fully tight condition is presented in Figure 18. In the next step, bolt D6 was loosened by 1/6 of a full turn (all other bolts are tight). This is just enough for the bolt

not to have a force preventing the threads from slipping; i.e. bolt can turn with minimal force. The same excitation signal was applied to sensor S7. The pulse of an elastic wave travelled through the joint was measure with S6. The record of the elastic wave corresponding to loosened bolt D6 condition is shown in Figure 18.

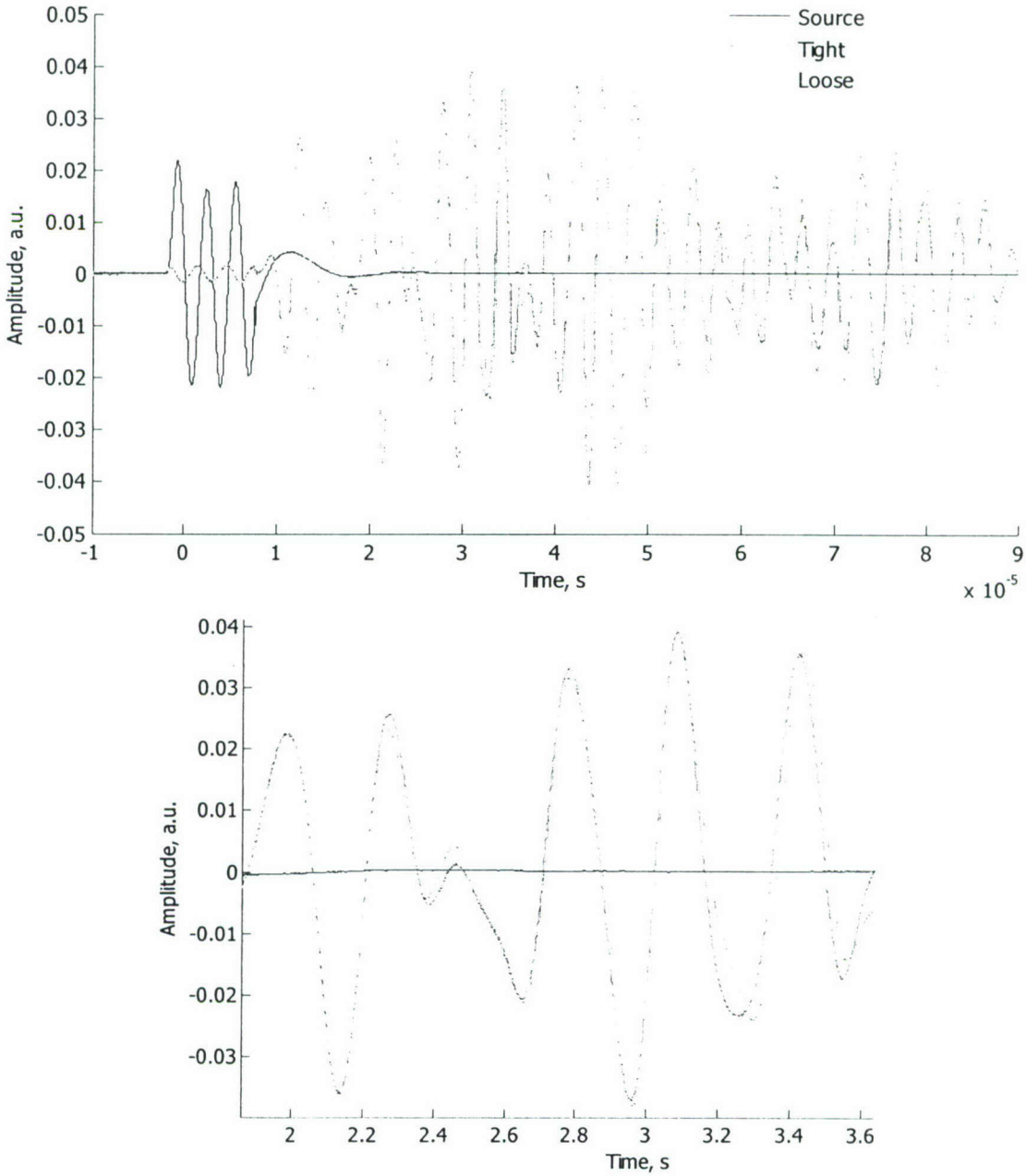

Figure 18 Elastic wave signals in the satellite panel experiment: black – transmitted pulse, blue – tight condition for neighboring bolts, red – loose condition – one bolt is loosened. The inset indicates phase shifts due to loose and tight test scenarios.

Examination of Figure 18 reveals that the elastic wave record is an assembly of pulse trains especially early in time. Individual pulses in a train are attributed to reflection and transmission of elastic wave through certain interfaces. The iso-grid of the panel is a periodic structure and hence it produces repeatable pattern of reflections. This is observed in Figure 18 where the first pulse corresponds to directly transmitted signal and the second pulse is likely due to reflection from corners of the iso-grid element. Noticeable, the first pulse shows practically no difference between tight and loose conditions because the wave propagates through a center of the iso-grid. This central location sees very little effect of stress induced by neighboring bolts. The second pulse is most likely coming from corners of the iso-grid quadrants subjected to stress from neighboring bolts. As a result, the record starts to show a phase shift for the tight condition. Further shifts are observable in subsequent pulses. The results of this experiment support feasibility of the acousto-elastic technique in monitoring complex structural elements such as satellite panels.

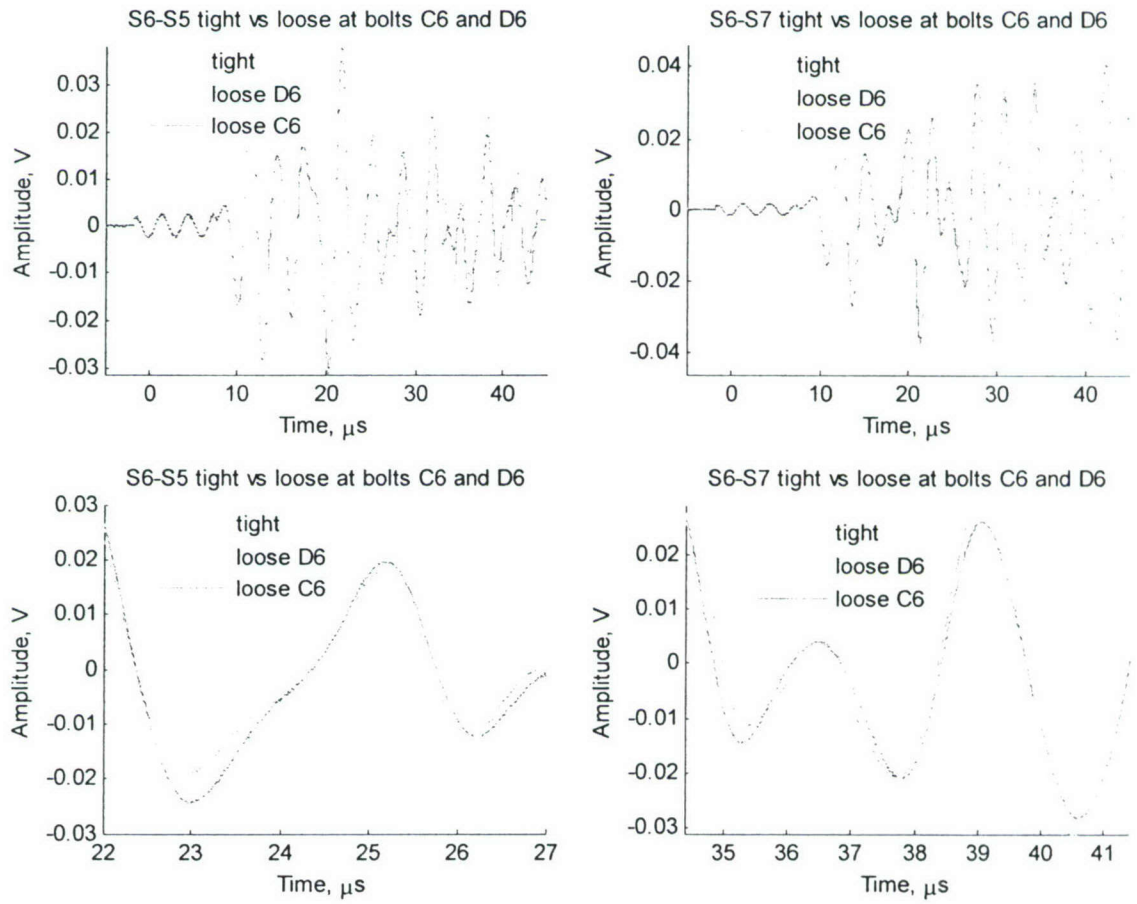

Figure 19 Elastic wave signals in the damage location experiment on the satellite panel: left - results for the sensor set S6-S5 and zoomed-in portion of the signal; right - results for the sensor set S6-S7 and zoomed-in portion of the signal.

An additional experiment was conducted to demonstrate capability of the acousto-elastic method to determine location of the loosened bolt. Sensor S5 was installed in a center of the iso-grid quadrant neighboring bolts D6 and C6 as indicated in Figure 17. This allowed for conducting experiments with two sets of sensors: S5-S6 and S6-S7. The difference between these sets is that distance between S5 and S6 is a little less than 2 inches and the set S6-S7 is located next to the edge of the panel. However, in both sensor sets bolts were positioned symmetrically to the line of the wave propagation. Left portion of Figure 19 shows the S5-S6 data for the cases when all bolts were tight, bolt C6 was loosened, and bolt D6 was loosened. Since bolts are positioned symmetrically with respect to a line connecting sensors, we anticipated responses that match closely. This is indeed observable in Figure 19 for time instants before 30 μs. After this time, responses deviate slightly due to possible misalignment of the sensor from the iso-grid centerline. Both responses show features that allow to distinguish "tight" and "loose" conditions. Right portion of Figure 19 shows the S5-S6 data for the cases when all bolts were tight, bolt C6 was loosened, and bolt D6 was loosened. For this case, bolt C6 is not symmetric with respect to the sensor line and is situated much further away. As a result, in Figure 19 we observe that loosening of D6 cases the difference in responses after the end of the second pulse (also consistent with results depicted in Figure 18), but loosening of C6 leads to changes noticeable much later – after a third pulse. Before 35 μs the data corresponding to loosened C6 show similarity with "tight" condition. Therefore, we conclude that by examining onset of the phase changes in the signal, it is possible to determine location of the loosened bolt.

We suggest that the data reported in this section of the report indicates feasibility of the acousto-elastic ENU SHM techniques for monitoring integrity of a complex structure such as a satellite panel. Further studies will be directed towards optimizing this technique for particular structural elements and improving understanding of reflection process from the iso-grid features.

6 ENU SHM OF EPOXY BONDS

In this section, we discuss application of embedded nonlinear ultrasonics for monitoring integrity of epoxy bonds. Two types of specimens are investigated: thin-walled plates bonded with Hysol® EA 9309NA epoxy and aluminum honeycomb panel.

6.1 ENU Monitoring of Thin-Walled Aluminum Plates Bonded with Hysol® Epoxy

To investigate performance of embedded nonlinear ultrasonics in monitoring integrity of epoxy bond, we considered thin aluminum plates bonded Hysol® EA 9309NA epoxy. Details on the specimens can be found in one of the preceding sections of the report. Sensors were positioned 1" away from the bond. In addition, for several specimens, data were acquired with an additional sensor positioned 2" from the far end of the plate. Configuration of the samples and sensor layout are presented in Figure 20.

Experiments of two types were carried out for specimens with epoxy bond: a long pulse experiments and short pulse experiments. Both approaches were aimed at assessing the level of nonlinearity associated with good and bad bonds.

6.1.1 Long Pulse Nonlinear Measurements of Epoxy Bond

Advantage of using long pulses (quasi CW excitation) consists of approaching the infinite waveform criterion essential for adequate application of Fourier analysis. The longer the record, the better frequency resolution can be achieved in the spectrum. In nonlinear measurements, additional benefit of using a quasi CW mode is associated with a notion that high power (in comparison with a short pulse) delivered by CW excitation affects magnitude of nonlinear interaction and leads to more pronounced manifestation of nonlinear effects. The Ritec measurement system allowed for transmitting 200 μs harmonic bursts. Frequency of the carrier was selected within 250 kHz – 350 kHz range. Initially, we conducted experiments with samples representing extreme cases: intact bond and 1" (area) disbond. A traditional nonlinear acoustic approach consisting of correlating amplitudes of higher harmonic with potential loss of structural integrity was considered first. A long pulse of 270 kHz was utilized as an excitation signal. Results of this experiment are presented in Figure 21 on dB re 1 V_{pp} scale. The figure provides a comparison of spectral data obtained from the good bond (GE3), the bad bond with a sensor located near the joint (BE3 – measured with S_3) and the bad bond with a sensor located far away from the joint (BE4 – measured with S_4). The distance between S_3 and S_4 was approximately 7 inches. The figure indicates a substantial level of higher harmonics associated with the nonlinear behavior. Amplitudes of second harmonic differ in 10 dB for the good and bad bonds. The difference reaches more than 25 dB (20 times) for third and fourth harmonics. Such a high level of higher harmonics may reflect substantial contribution of the acoustic nonlinearity in the joint. However, the disadvantage of the classical nonlinear acoustic method presented above is that equipment nonlinearities inherent in the experimental setup also contribute to amplitudes of the high harmonics. To address this issue, we employed a modulation method [14, 18] based on dual frequency CW excitation. The advantage of the modulation method is that nonlinear

interaction of the elastic waves occur only in the structural component and thus is manifested at sum (f_1+f_2) and difference (f_2-f_1) frequencies. In this case, equipment nonlinearity contributes only into spectral amplitude of 2nd, 3rd, etc. harmonics. The excitation signals for the modulation experiment were long pulses of 270 kHz (S_1) and 350 kHz (S_2). Figure 22 presents results of the modulation experiment. Noticeable in the figure, spectral amplitude of the sum frequency for the intact bond is negligibly small. In contrast, spectral amplitude of the sum frequency for the specimen with a disbond approaches -40 dB, which gives approximately -25 dB difference for good and bad bonds. Encouraged by results obtained for extreme cases, we fabricated two additional specimens featuring disbonds of incrementally smaller sizes: specimen E1` contained a disbond of approximately 0.2 $in^2$ and specimen E2` contained a disbond of 0.4 in^2. Only one pair of sensors was installed on each additional specimen to implement the traditional nonlinear acoustic approach based on measurement of spectral amplitudes of higher harmonics. The measurement results for four specimens including the intermediate cases are presented in Figure 23. The normalized spectrum again reveals substantial difference between the intact and the largest damage. The second harmonic shows little difference between intact and intermediate damage cases. It suggests a noticeable change for the case of large damage. Spectral amplitude of the third harmonic shows proportionality with the level of damage. This still is retained to a certain extend in the data for the forth harmonic. Summarizing experimental results for the long pulse experiment, we suggest that spectral features reflecting the system's nonlinearity may be used to discriminate good and bad bonds. However, a range of effects including contributions of the bond thickness and frequency response of the sample needs to be clarified before using the long pulse technique.

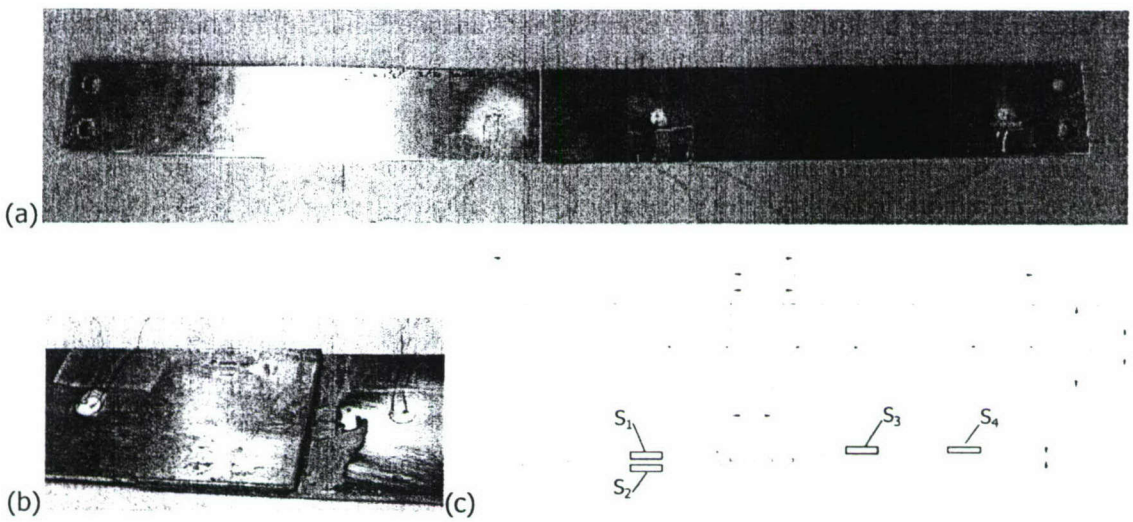

Figure 20 Illustration of epoxy bond specimen: (a) 12"×2" aluminum plates bonded with 1.5" overlap, (b) close-up showing position of sensors, (c) details of the sensor layout for dual frequency experiments.

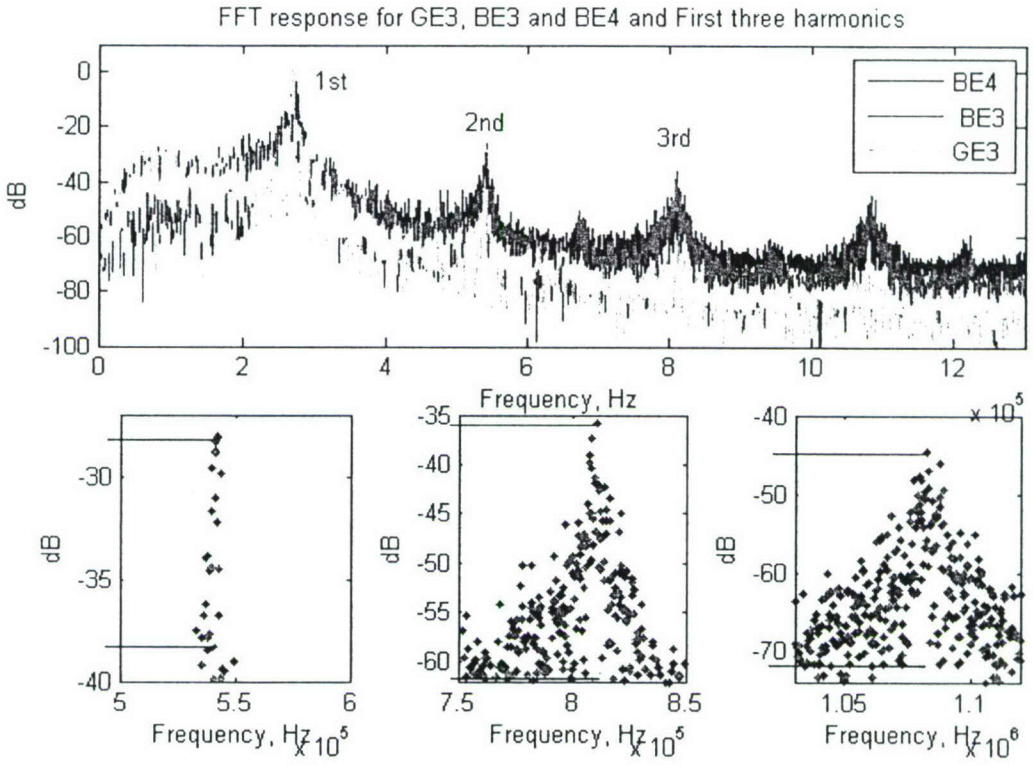

Figure 21 Spectral characteristics of good (GE3) and bad (BE3 and BE4) bonds in a single frequency long pulse experiment.

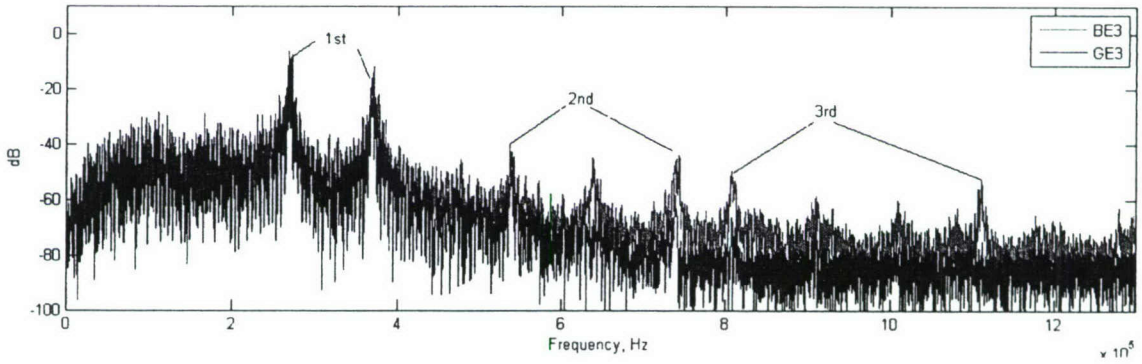

Figure 22 Spectral characteristics of good (GE3) and bad (BE3) bonds in dual frequency long pulse modulation experiment.

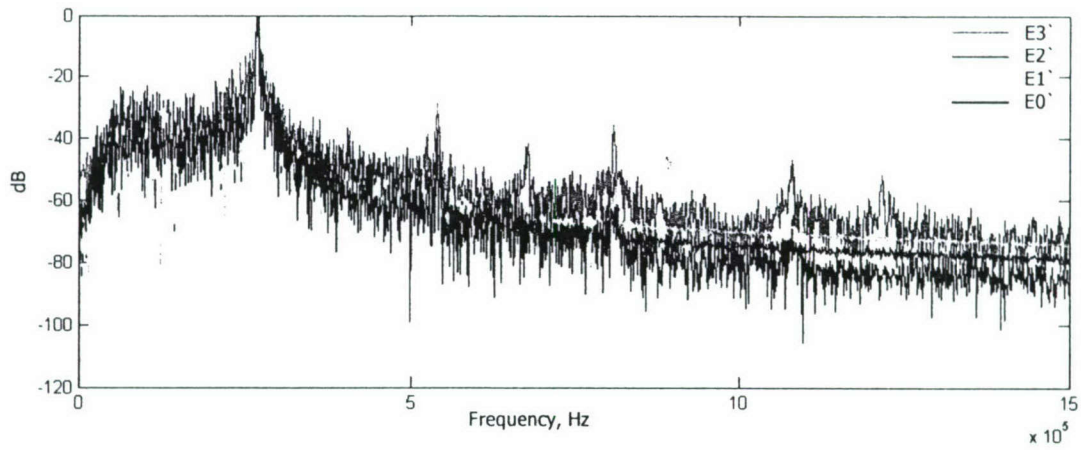

Figure 23 Spectral characteristics of samples with different epoxy bond quality: E0` - intact bond, E1` - a bond with disbonded area of 0.2 in^2, E2` - a bond with disbonded area of 0.4 $in^2$, E3` - a bond with disbonded area of 1 in^2.

6.1.2 Short Pulse Nonlinear Measurements of Epoxy Bond

In this section we describe an embedded nonlinear ultrasonic method developed in our laboratory to enable nonlinear measurements with short pulses. One of the main reasons for developing such a method is reducing effect of the sample's frequency response on nonlinear measurement. When a long pulse or CW wave is transmitted to a specimen, it sets up vibrations at frequencies available in the excitation signal. This is, to a certain extend, is equivalent to a multi-sine excitation with one dominant frequency and harmonics of smaller amplitude. Because "linear" vibration modes are excited at these frequencies, they contribute into spectral amplitude of nonlinear components in the spectrum of the received signal. This process may increase or decrease spectral amplitudes associated with nonlinearity. To mitigate this problem two options are suggested: (a) utilize an averaging procedure over the frequency band [14] or normalize nonlinear measurements by "linear" frequency response, which is a challenging task at high frequencies. From a practical point of view, the first approach is the most plausible. Alternatively, a method is suggested that avoids a direct excitation of vibration modes by employing a short pulse rather than CW signal.

The proposed method explores differences in structural response to an elastic wave pulse signal at different amplitude levels. In the linear system, increase of amplitude results in a signal of higher power, but the same type (shape). For a harmonic signal this means that temporal position of the peak amplitude is independent on the amplitude level. In contrast, in the nonlinear system, temporal position the peak amplitude depends on the amplitude level. For example, when a sinusoidal signal changes into a nonlinear saw-tooth wave, temporal position of the maximum shifts. This effect is explored in the proposed ENU SHM method.

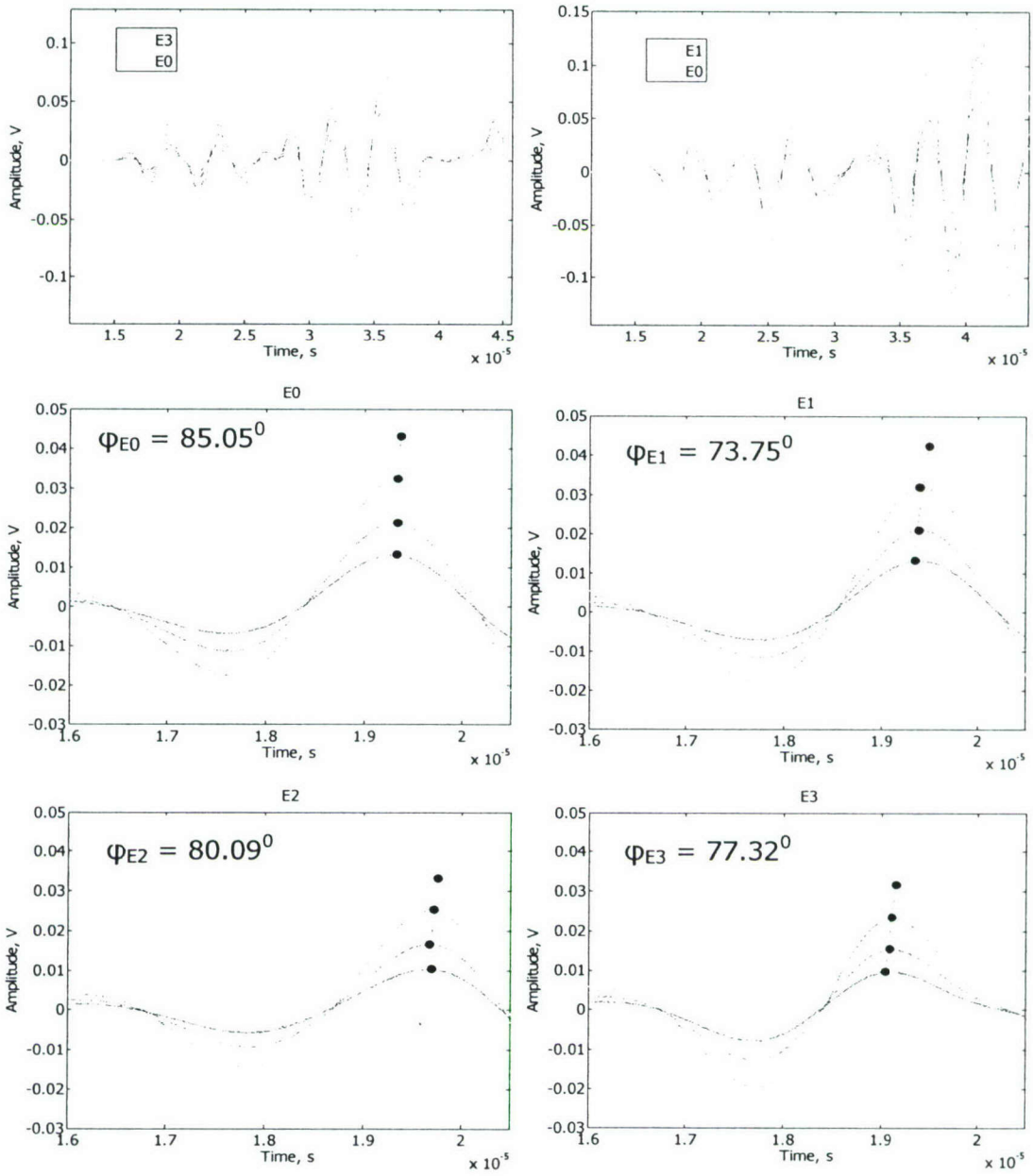

Figure 24 Results of a short pulse experiment for samples of epoxy bond with various level of damage: E0-intact, E1-minor damage, E2-medium damage, E3-severe damage.

A new set of samples was fabricated to support short pulse ENU measurements. Dimensions of the samples were identical to aluminum plates discusses in the preceding section (12"×2"), but only rectangular disbonds were considered. The disbonds had the same length of 1 in (along the length of sample), but progressively decreasing widths of 1", 0.5", and 0.25 in. All specimens were bonded with Hysol® EA 9309NA epoxy. The fabrication process resulted in specimens with the following damage: E0 – intact (no damage), E1 – minor disbond of 0.25 in^2, E2 – medium disbond of 0.5 in^2, and severe disbond of 1 in^2. Disbonds were created by leaving a portion of material not covered with epoxy. Piezoelectric wafer active sensors were installed 1 inch away from the edge of a bond on a surface of each aluminum plate. During experiments, a 3 count 270 kHz signal of progressively increasing amplitude was supplied to a transmitting sensor. The response signal was measured with the second sensor and digitized by NI 5142 digitizer. Upper portion of Figure 24 shows examples of records obtained from specimens E0, E1, and E3. After a signal was recorded, a Matlab® code was used to smooth signals via averaging and find maximums of the first well-pronounced peak in the record. These maximums for all four specimens are indicated with black markers in Figure 24. Position and magnitude of the amplitude maximums allowed for calculating the best linear fit for these data points. A line representing the best fit of the maximums is also presented in Figure 24 for each damage scenario. Analysis of the figure reveals that the case of intact epoxy bond shows almost a vertical line connecting the maximums. For all damaged samples, this line is noticeably tilted. To quantify the tilt, we calculated an inclination angle with respect to time axis and presented results in Figure 24. The intact sample shows a tilt angle of 85^0, sample with minor damage shows the largest tilt of 74^0, sample with medium damage shows 80^0, and sample with largest disbond shows 77^0. Although all damaged samples revealed considerable difference from the intact case, correlation between the damage size and amount of tilt is not transparent. According to experimental data, the smallest damage resulted in the largest tilt angle. Except this data point, however, the tilt angle correlates with the damage size. A few issues need to be noted in respect to this situation. First, our estimation is based on one set of data, which is subject to a statistical deviation with currently unknown parameters. More data sets are needed to determine statistical variation of the measurement values. Second, it has been shown [33] that thickness of the bond may contribute substantially to magnitude of the nonlinear response. Since thickness of the epoxy layer was not monitored during fabrication process, there is a possibility of having samples with different bond thicknesses. In fact, it is difficult to estimate fabrication inconsistencies and magnitude of their contribution into the nonlinear response. This is a subject of further investigations.

We conclude that the suggested short pulse ENU technique is a promising candidate for damage detection in epoxy bonds. However, because the technique is in its infancy, it needs further refinements and adjustments based on requirements in practical applications and structural assessment scenarios.

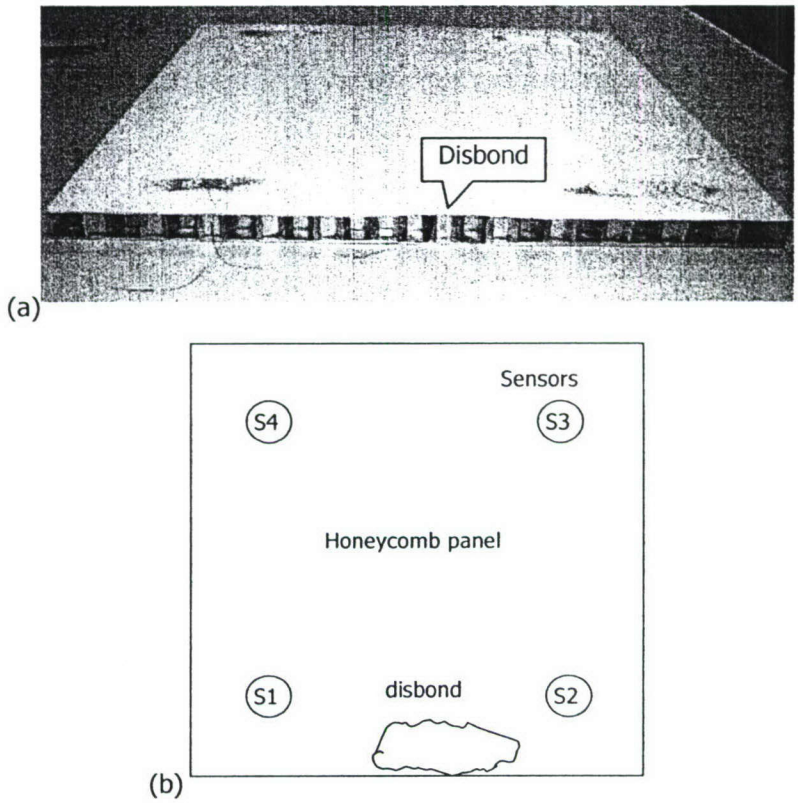

Figure 25 Aluminum honeycomb panel used in experiments: (a) a photograph of the panel showing location of a disbond, (b) layout of sensors on the panel.

6.2 Aluminum Honeycomb Panel

An aluminum honeycomb panel was utilized as a realistic example of a complex structural element bonded with epoxy. A disbond was introduced from edge of the plate using a spreader bar. While exact extend of damage is unknown, a crack of approximately 6 cm is observable from the side of a panel. The panel was painted by manufacturer and the paint was sanded from portions of the panel before installing piezoelectric sensors. A photograph of the panel and a diagram showing position of sensors are presented in Figure 25. Further details on this experimental specimen can be found in section 3 of this report.

6.2.1 Long Pulse Nonlinear Measurements in Honeycomb Panel

A nonlinear acoustic approach based on measuring spectral amplitudes of higher harmonics was investigated for damage detection in aluminum honeycomb panel. A 200 μs harmonic pulse signal of frequency 350 Hz was supplied to a piezoelectric sensor configured for transmitting the elastic wave. Such a long pulse essentially establishes quasi CW excitation of the panel as the wave reflects many times from boundaries. The propagated wave was received by another sensor. Six configurations were explored: sensor pairs on each side of the panel and two diagonal pairs. The measurement results are presented in Figure 26 for each sensor pair. Two spectrums on one plot corresponds to one sensor being a transmitter and another a receiver and vice versa. A reader needs to note that sensors S1 and S2 is a

sensor pair near the disbond. Sensor S3 and S4 are on the far side of the panel opposite the disbond. According to Figure 26, this sensor pair shows little evidence for presence of nonlinearity as only a third harmonic is detectable. Similar situation is observable for pairs S1-S4 and S1-S3. However, all spectra featuring S2 show distinctively different picture. A second harmonic at approximately – 75 dB appear when S2 works as a transmitter. While the origin of such a behavior is open to speculation, we considered quality of sensor installation as the most probable cause of spectral discrepancy. As a result, the data was disregarded and sensor S2 was replaced with a new one.

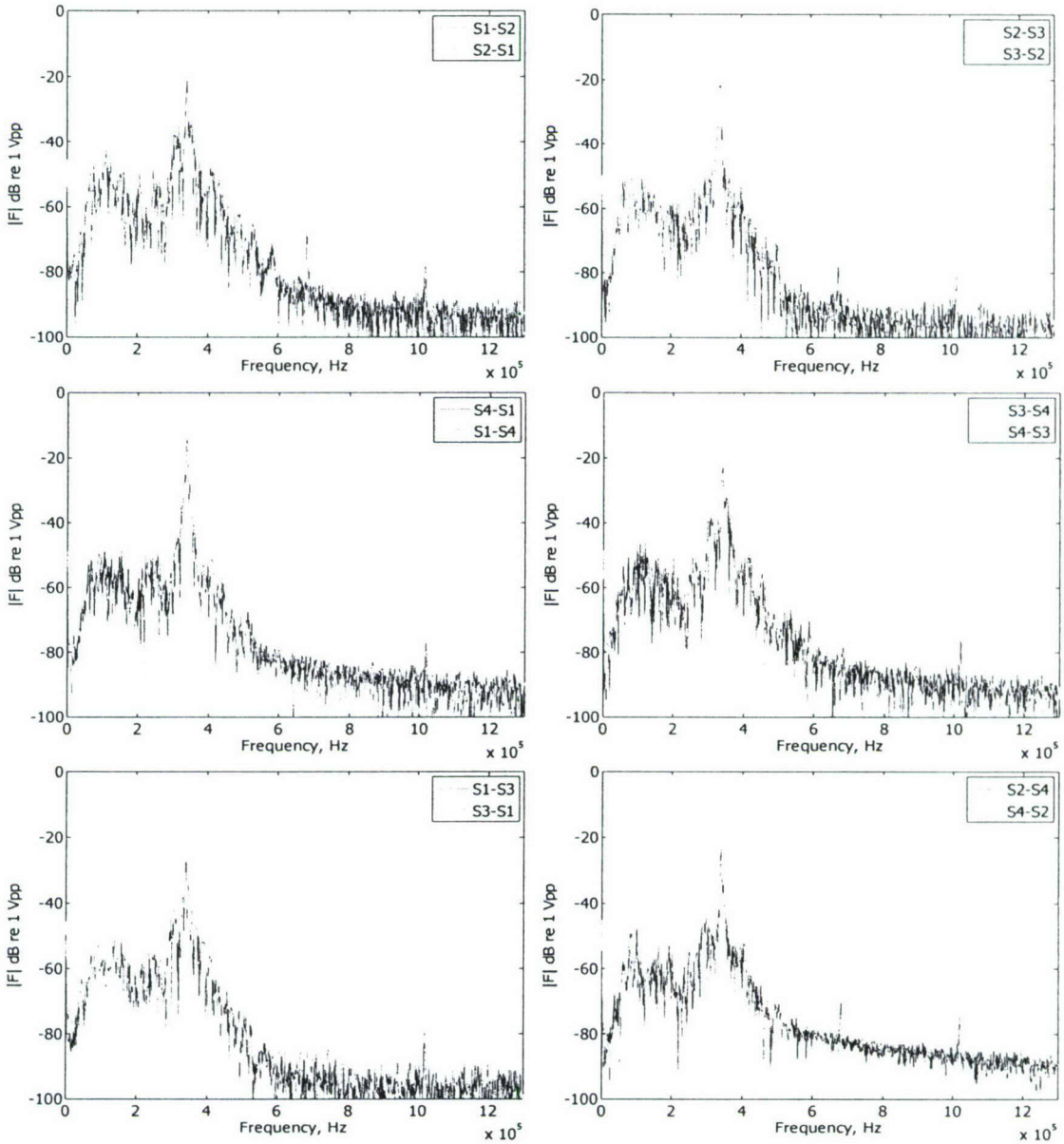

Figure 26 Spectral characteristics of signals measured in the long pulse experiment on a honeycomb panel.

6.2.2 Short Pulse Nonlinear Measurements in Honeycomb Panel

Encouraged by success of the short pulse technique in detecting disbonds in aluminum specimens, we considered its application to assessment of the disbond in the honeycomb panel. For this reason, old sensor S2 was replaced with a new one.

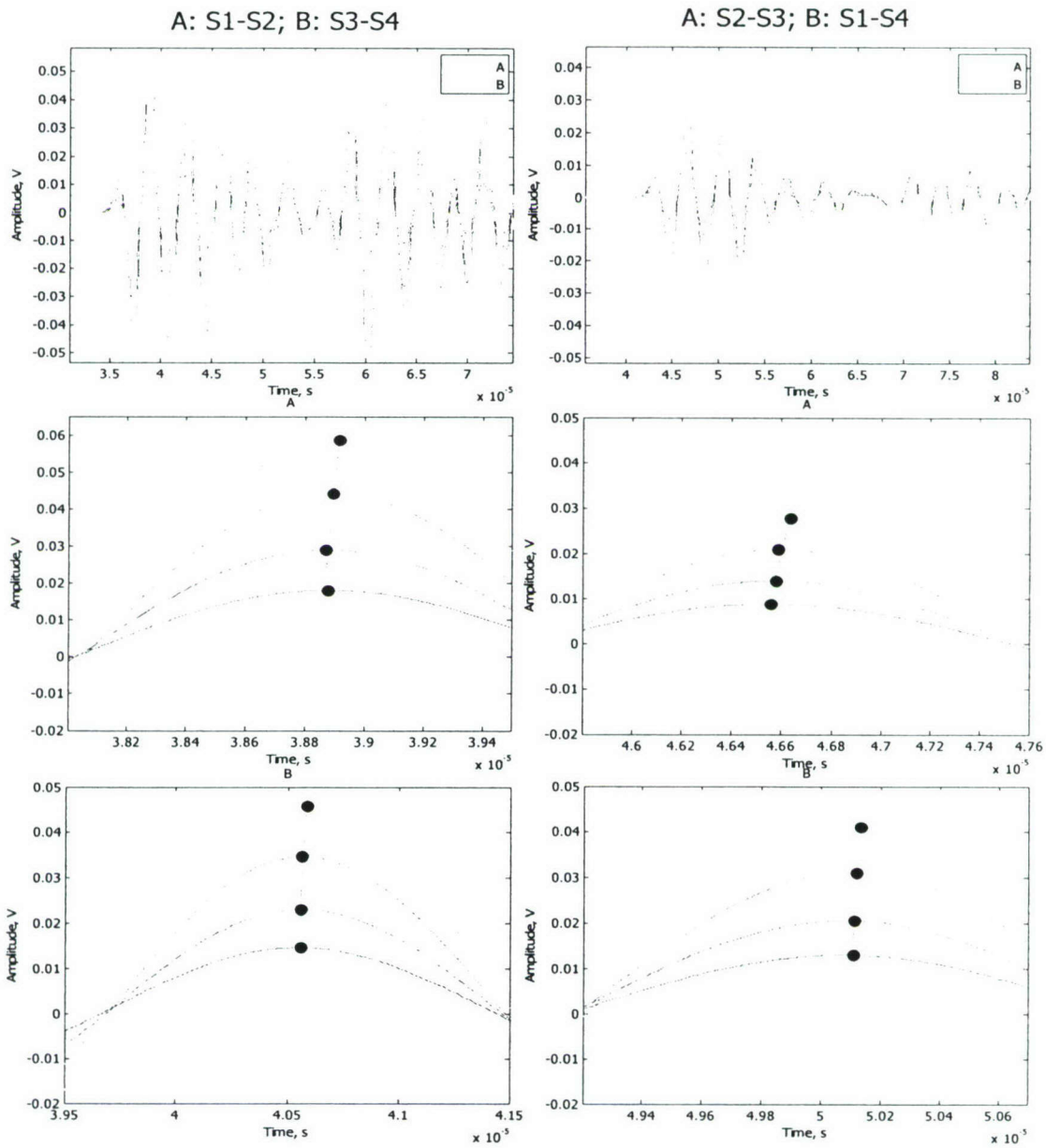

Figure 27 Results of a short pulse experiment on a honeycomb panel: sensor pairs S1-S2, S3-S4, S2-S3, S1-S4.

A three count 320 kHz pulse was transmitted and received by sensors configured in previously reported sensor pairs. Excitation amplitude was increased incrementally to facilitate evaluation of relative changes in temporal position of amplitude maximums. This resulted in four sets of data for each sensor pair. The data was grouped according to sensor position: S1-S2 (near damage) and S3-S4on the opposite side, two pairs on left and right sides of the panel S2-S3 and S1-S4, and diagonal pairs S4-S2 and S3-S1. Graphical representation of the data for discussed sensors is available in Figure 27and Figure 28.

In one of preceding sections we described the algorithm for evaluating position of signal maximums with respect to time axis. This algorithm was applied to the data measured on the honeycomb panel and the lines indicating the signal tilt were calculated. From Figure 27 and Figure 28 we infer that sensor pairs S3-S4, S1-S4, and S3-S1 produced the smallest tilt while pairs S1-S2, S2-S3, and S4-S2 produced noticeable inclination. One of largest inclinations was measured for the sensor pair S2-S3. The new set of data raised questions similar to those considered in the long pulse experiment. Specifically, what might cause a high level of nonlinearity in signals associated with sensor S2? Previously, we considered inadequate installation as the most probable reason for spectral discrepancies in Figure 26. However, a new sensor through a very different technique shows comparable results. It is interesting to note that one of largest tilts was observed for the case when S2 was acting as a transmitter, similar to cases in Figure 26. In addition, it is the only sensor which shows such a behavior, even when replaced. It is possible that either deficiencies in the internal structure

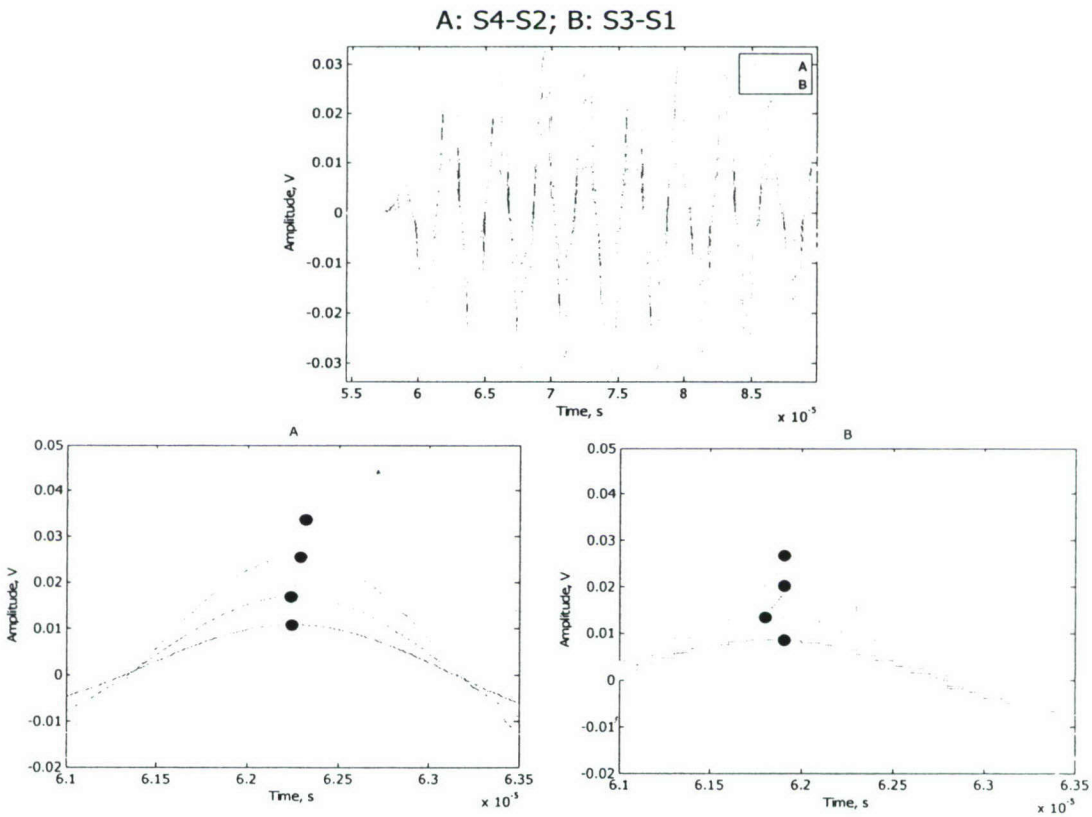

Figure 28 Results of a short pulse experiment on a honeycomb panel: diagonal sensor pairs S4-S2, S3-S1.

of a panel or damage propagated towards S2 is causing high level of nonlinearity in responses associated with S2. This assumption, however, is difficult to verify without disassembling a panel and inspecting region next to S2. At this point, we suggest that it may be possible to use the short pulse technique for assessment of structural damage in complex structures, but additional work is needed to establish benchmark measurements for this technique and to improve understanding of the nonlinear process in complex structures.

7 CONCLUSIONS

This report discussed application of the embedded nonlinear ultrasonics for monitoring integrity of complex aerospace structures. The research efforts were focused on developing methods for assessing structural joints as critical elements of structural assembly. We considered bolted joints and epoxy joints. Two methods were explored for evaluating integrity of bolted joints: the acousto-elastic method and the modulation method. In the acousto-elastic method, the torque applied to bolts was estimated based on the delay of the elastic wave caused by stressing of the structural material. Changes of the pulsed propagation time due to perpendicularly applied stresses were in the range of 0.1 – 0.6 μs. We conducted 40 experiments to determined statistical variation of the pulse arrival time under various levels of torque. Five torques were selected (10, 20, 30, 40, and 50 ft-lbs) and eight measurements for each torque level were conducted. Results of experiments show linear dependence of the arrival time on the applied torque. The proposed technique can be used not only to evaluate a binary scenario (torque/ no torque), but also to quantify the amount of torque applied to the joint. Accuracy of the method was noticeably better at high torque values, but it decreased at very low torques where larger scattering of data was observed.

Acousto-elastic theory was applied to estimate changes of the sound speed due to stresses exerted by bolts. A conventional modeling approach was utilized that considers a longitudinal wave propagating in an infinite medium. One order of magnitude underestimates were obtained from the theory. Such level of underestimates is not surprising due to differences in material parameters, difficulties in determining exact extent of stresses, and utilizing a sound speed formulation for the infinite medium. The actual sound speed in an aluminum plate is lower, which implies that a propagating pulse experiences more static stress from the joint. Hence, it is natural to obtain larger pulse delays in the experimental study.

In the modulation experiment, long 200 μs pulses of different frequencies (270 kHz and 370 kHz) were used to study the effect of the applied torque on the signal spectrum. The response of the joint was measured in two locations: next to the joint and further away from the joint. Both spectra show higher level of spectral components in 'tight" condition. However, this technique is difficult to apply consistently because frequency response of the specimen affects amplitudes of measured frequencies. An averaging technique is recommended to address this issue.

A realistic satellite panel was fabricated from aluminum plates to study applicability of ENU for monitoring bolted joints in complex structures. Each plate featured an iso-grid construction and 49 holes for housing bolts. Piezoelectric sensors were positioned in separate iso-grid quadrants. After all bolts were tightened, a 3 count 270 kHz pulse was applied to one sensor and the response was measured by the sensor on the other side of the iso-grid. Then one of the nearby bolts in a corner of the iso-grid was loosened to the point of slipping and the elastic wave signal was recorded. The data shows a noticeable phase shift of the signal reflected from stressed portions of the structure. This phase shift can be used for quantifying torque levels in the panel and locating loosened bolts.

Three nondestructive evaluation methods were employed for monitoring integrity of epoxy bonds: a traditional nonlinear acoustic method based on assessment of spectral amplitudes of higher harmonics, the dual-frequency excitation modulation method and a new short pulse method, which evaluates temporal shift of signal maximums at different excitation amplitudes. All methods have shown good performance in detecting relatively large disbond in thin-walled aluminum specimens. However, although detected, damage of smaller size produced mixed results preventing straightforward classification. It is believed that deviation of the bond thickness and other fabrication inconsistencies may contribute into classification errors.

Similar methods (except modulation) were applied to detection of a disbond in aluminum honeycomb panel. Preliminary data based on measurements of higher harmonics revealed elevated spectral amplitudes for responses containing a particular sensor (S2). This data was initially disregarded because inadequateness of the sensor installation was considered as primary cause of nonlinearity. The sensor was replaced with a new one and a short pulse method was applied for locating the disbond. Remarkably, this new method produced results comparable to preliminary data with sensor S2 responses indicating presence of nonlinearity. Deficiencies of the internal structure of the panel and damage propagated towards S2 were cited as possible causes of high level of nonlinearity in measured responses. We suggest that the short pulse technique is a promising candidate for assessment of structural damage in complex structures, but additional work is needed to transit this technology to practical applications. In addition, developing of in-depth understating of physical phenomena governing nonlinear processes in complex structures is essential for practical application of nonlinear ultrasonics SHM methods.

8 ACKNOWLEDGMENTS

Authors would like to acknowledge Air Force Office of Scientific Research for funding this study and program manager Dr. Victor Giurgiutiu for valuable insights and advice during the course of the project. Our deep gratitude is to AFRL/RVSV, Kirtland Air Force Base and Mr. Brandon Arritt, deputy program manager of Integrated Structural Systems and Symbiotic Structures, for supporting and guiding reported research activities.

9 REFERENCES

1. Sohn, H., Farrar, C.R., Hemez, F.M., Shunk, D.D., Stinemates, D.W., and Nadler B.R., (2004) "A Review of Structural Health Monitoring Literature: 1996–2001," Los Alamos National Laboratory Report, LA-13976-MS, 2004.
2. Raghavan, A. and Cesnik, C.E.S. (2005) "Piezoelectric-actuator excited-wave field solutions for guided-wave structural health monitoring," *Proceedings of SPIE on Sensors and Smart Structures Technologies for Civil, Mechanical, and Aerospace Systems*, Vol. 5765, p 313-323.
3. Ihn, J.B., and Chang F-K., (2004) "Ultrasonic Nondestructive Evaluation for Structural health Monitoring: Build-in Diagnostics for Hot-spot Monitoring in Metallic and Composite Structures," in *Ultrasonic Nondestructive Evaluation: Engineering and Biological Material Characterization*, edited by T. Kundu, CRC press 2004.
4. Lemistre, M., Osmont, D., and Balageas, D., (2000) "Active Health System Based on Wavelet Transform Analysis of Diffracted Lamb Waves," *Proceedings of SPIE on Fifth European Conference on Smart Structures and Materials*, Vol. 4073, pp. 194–202.
5. Giurgiutiu, V., Bao, J., and Zhao, W., (2003) "Piezoelectric Wafer Active Sensor Embedded Ultrasonics in Beams and Plates," *Experimental Mechanics*, Vol. 43, No. 4, 428–449.
6. Mal, A. K., Ricci, F., Gibson, S., and Banerjee, S., (2003) "Damage Detection in Structures from Vibration and Wave Propagation Method," *Proceedings of SPIE on Smart Nondestructive Evaluation and Health Monitoring of Structural and Biological Systems II*, Vol. 5047, pp. 202–210.
7. Lee, B. C. and Staszewski, W. J., (2003) "Modeling of Lamb Waves for Damage Detection in Metallic Structures," Smart Materials and Structures, Vol. 12, 804–814.
8. Lin, X. and Yuan, F. G., (2005) "Experimental Study of Applying Migration Technique in Structural Health Monitoring," *Structural Health Monitoring – An International Journal*, December 2005; 4: pp. 341 - 353.
9. Kleiman, M.P., (2006) "Responsive, Flexible, and Affordable Satellite," www.afrlhorizons.com, October 2006.
10. Cantrell, J.H., Yost, W.T. (2001) "Nonlinear Ultrasonic Characterization of Fatigue Microstructures" International Journal of Fatigue, n 23, pp. S487-S490.
11. Frouin, J., Sathish, S., and Na, J.K. (2000) "Real-Time Monitoring of Acoustic Linear and Nonlinear Behavior of Titanium Alloys During Low-Cycle Fatigue and High-Cycle Fatigue" Proceedings of the SPIE's 5th International Symposium on Nondestructive Evaluation and Health Monitoring of Aging Infrastructure, Vol. 3993, pp 60-67.
12. Guyer, R.A. and Johnson, P.A. (1999) "Nonlinear Mesoscopic Elasticity: Evidence for a New Class of Materials," Physics Today, Vol. 52, pp 30-35.
13. Van Den Abeele, K.E., Carmeliet, J., Ten Cate, J.A. and Johnson, P. A., "Nonlinear Elastic Wave Spectroscopy (NEWS) techniques to discern material damage, Part II: Single Mode Nonlinear Resonance Acoustic Spectroscopy," *Research in Nondestructive Evaluation*, Vol. 12, n. 1, 2000, pp. 31-42.
14. Donskoy, D., Sutin A., and Ekimov A. (2001) "Nonlinear Acoustic Interaction on Contact Interfaces and its use for Nondestructive Testing", *NDT&E International*, Vol. 34, pp. 231-238, 2001.
15. Kim, J.-Y., Yakovlev, V. A. and Rokhlin, S. I. (2004) "Surface acoustic wave modulation on a partially closed fatigue crack," *Journal of the Acoustical Society of America*, Vol. 115, pp 1961-1972.
16. Rokhlin, S.I., Wang, L., Xie, B., Yakovlev, V.A, Adler, L., (2004) "Modulated angle beam ultrasonic spectroscopy for evaluation of imperfect interfaces and adhesive bonds," Ultrasonics Vol. 42, pp. 1037–1047.
17. Masuda, A., Yonemura, Y., Sone, A., (2006) "Active Sensing and Characterization of Nonlinear Damages by Modulated Phases and Envelopes of Scattered Waves," *Proceedings of SPIE 11th Symposium on Sensors and Smart Structures Technologies for Civil, Mechanical, and Aerospace Systems*, Vol. 6175, 26 Feb. – 2 March 2006, San Diego, CA.

18. Zagrai, A., Donskoy, D., Chudnovsky, A., Golovin, E., (2006) "Nonlinear Acoustic Structural Health Monitoring," *Proceedings of 47th AIAA/ASME/ASCE/AHS/ASC Structures, Structural Dynamics, and Materials Conference*, Newport, RI, 2006, paper 106-SDM-67.
19. Todd, M.D., Chang, L., Erickson, K., Lee, K., Nichols, J.M., (2004) "Nonlinear excitation and attractor mapping for detecting bolt preload loss in an aluminum frame," *Proceeding of SPIE's Conference on Health Monitoring and Smart Nondestructive Evaluation of Structural and Biological Systems III*; Vol. 5394, pp. 317-328.
20. Adams, D.E. and Nataraju, M. (2002) "A Nonlinear Dynamical Systems Framework for Structural Diagnosis and Prognosis," International Journal of Engineering Science, Volume 40, Issue 17, October 2002, pp. 1919-1941.
21. Epureanu, B.I. , Shih-Hsun Yin, S.-H., and Derriso, M.M. (2005) "High-Sensitivity Damage Detection Based on Enhanced Nonlinear Dynamics," Smart Materials and Structures, 14, pp. 321-327.
22. Jhang, K.Y., Quan, H.H., Ha, J., Kim, N.Y., (2006) "Estimation of clamping force in high tension bolts through ultrasonic velocity measurement," Ultrasonics, Vol. 44, pp el339-el342.
23. Yang, J., Chang, F., (2006) "Detection of bolt loosening in C–C composite thermal protection panels: II. Experimental verification," Smart Materials and Structures, Vol. 15, pp. 591-599.
24. Light, G.M., Ruescher, R.H., Bloom, E.A., Joshi, N.R., Tsai, Y.M., Liu, S.N., (1993) "Application of the cylindrically guided wave technique for bolt and pump shaft inspections," Nuclear Engineering and Design, Vol. 144, pp. 465-468, Elsevier Science Publishers.
25. Couchman, J., Bell, J., Noronha, P., (1976) "Computerized signal processing for detecting cracks under installed fasteners," Ultrasonics, pp 256-262.
26. Beyer, R.T. (1974) Nonlinear Acoustics, Published by Acoustical Society of America in 1997.
27. Zarembo, L.K. and Krasil'nikov, V.A. (1971) "Nonlinear Phenomena in the Propagation of Elastic Waves," Sov. Phys. Usp., 13, pp. 778-797.
28. Norris, A.N., (1997) "Finite-Amplitude Waves in Solids," in Nonlinear Acoustics edited by Hamilton, M.F. and Blackstock, D.T., Academic Press, 1997.
29. Thurston, R.N. and Brugger, K., (1964) "Third-order Elastic Constants and the Velocity of Small Amplitude Elastic Waves in Homogeneously Stressed Media," Phys. Rev. 133, A1604.
30. Budynas, R.G. and Nisbett, J.K. (2008) "Shigley's Mechanical Engineering Design," McGraw-Hill, 2008.
31. Nagy P.B. (2004), Course notes on Ultrasonic NDE.
32. Donskoy, D.M., and Sutin, A.M. (1998) "Vibro-Acoustic Modulation Nondestructive Evaluation Technique", Journal of Intelligent Material Systems and Structures, Vol. 9, September 1998, pp. 765-771.
33. Rothenfusser, M., Mayr, M., Baumann, J., (2000) "Acoustic Nonlinearities in Adhesive Joints," Ultrasonics, Vol. 38, pp.322-236.

10 APPENDIX A
STATISTICAL CHARACTERISTICS OF THE PULSE SIGNAL

10.1 Raw Data

The statistical data collected in 40 experiments (8 records for each torque level) are presented in Table 3. The data shows two outliers corresponding to the first two tests. Because of substantial difference between the outliers and the rest of data, we eliminated these points from further analysis.

10.2 Ranked Data

Table 4 contains the data in ranking order of signal finish time. That is the time it took to get to the second peak of the chosen signal section. Although the ranking is not entirely progressive from 1 to 8 there is a slight observance of increasing magnitude with time. This is most likely the result of plastic deformation on the specimen at 50ft×lbs of torque. To test this hypothesis, future studies will have to set the max torque much lower.

10.3 Statistical Classes

The number of statistical classes was determined according to the Sturgis Rule. This rule yielded a fractional number and we considered number 3 as the most adequate integer. Then the data lying between maximum and minimum of the signal arrival (finish) time were separated in three classes. A statistical frequency was determined and the Normal Distribution curve was calculated to facilitate comparison of distributions. Figure 29 illustrate results of calculations performed for different torque levels. It can be seen from the figure that majority of data follow normal distribution. The most significant deviations from the normal distribution curve are observed for minimum and maximum torque levels.

Table 3 Characteristics of the elastic wave signal measured for five values of torque.

10 FT*LBS		
TRIAL	START	FINISH
1	2.12127E-05	2.50127E-05
2	2.11427E-05	2.50627E-05
3	2.15959E-05	2.53759E-05
4	2.18093E-05	2.56493E-05
5	2.18981E-05	2.57281E-05
6	2.18467E-05	2.56467E-05
7	2.19444E-05	2.57944E-05
8	2.19561E-05	2.58161E-05
MEAN	2.16757E-05	2.55107E-05
STD	3.27807E-07	3.21959E-07
MEAN OMIT FIRST 2	2.18418E-05	2.56684E-05
STD OMIT FIRST 2	1.32897E-07	1.59779E-07

20 FT*LBS		
TRIAL	START	FINISH
1	2.13227E-05	2.50527E-05
2	2.13227E-05	2.50927E-05
3	2.21459E-05	2.58759E-05
4	2.20393E-05	2.57393E-05
5	2.21281E-05	2.60181E-05
6	2.21167E-05	2.57767E-05
7	2.21744E-05	2.58544E-05
8	2.21461E-05	2.58661E-05
MEAN	2.19245E-05	2.56595E-05
STD	3.73492E-07	3.71419E-07
MEAN OMIT FIRST 2	2.21251E-05	2.58551E-05
STD OMIT FIRST 2	4.6358E-08	9.66223E-08

30 FT*LBS		
TRIAL	START	FINISH
1	2.13827E-05	2.50927E-05
2	2.16927E-05	2.53627E-05
3	2.21159E-05	2.58259E-05
4	2.21093E-05	2.58693E-05
5	2.22381E-05	2.59481E-05
6	2.21967E-05	2.58967E-05
7	2.22344E-05	2.58844E-05
8	2.22661E-05	2.59561E-05
MEAN	2.20295E-05	2.57295E-05
STD	3.19609E-07	3.20708E-07
MEAN OMIT FIRST 2	2.21934E-05	2.58968E-05
STD OMIT FIRST 2	6.64143E-08	4.9163E-08

40 FT*LBS		
TRIAL	START	FINISH
1	2.15527E-05	2.51127E-05
2	2.20527E-05	2.57327E-05
3	2.21559E-05	2.58959E-05
4	2.22193E-05	2.59893E-05
5	2.22281E-05	2.60181E-05
6	2.22567E-05	2.59967E-05
7	2.23044E-05	2.59344E-05
8	2.23761E-05	2.60661E-05
MEAN	2.21432E-05	2.58432E-05
STD	2.57224E-07	3.12162E-07
MEAN OMIT FIRST 2	2.22568E-05	2.59834E-05
STD OMIT FIRST 2	7.60381E-08	6.05183E-08

50 FT*LBS		
TRIAL	START	FINISH
1	2.19327E-05	2.52127E-05
2	2.22327E-05	2.58827E-05
3	2.23059E-05	2.60259E-05
4	2.22893E-05	2.60893E-05
5	2.22781E-05	2.60781E-05
6	2.23467E-05	2.61267E-05
7	2.23244E-05	2.60544E-05
8	2.23061E-05	2.61261E-05
MEAN	2.2252E-05	2.59495E-05
STD	1.33331E-07	3.07721E-07
MEAN OMIT FIRST 2	2.23084E-05	2.60834E-05
STD OMIT FIRST 2	2.45655E-08	3.97702E-08

Table 4 Ranked data for the finish time of the elastic wave

10 FT*LBS		20 FT*LBS		30 FT*LBS	
TRIAL	FINISH (s)	TRIAL	FINISH (s)	TRIAL	FINISH (s)
1	2.50127E-05	1	2.50527E-05	1	2.50927E-05
2	2.50627E-05	2	2.50927E-05	2	2.53627E-05
3	2.53759E-05	4	2.57393E-05	3	2.58259E-05
6	2.56467E-05	6	2.57767E-05	4	2.58693E-05
4	2.56493E-05	7	2.58544E-05	7	2.58844E-05
5	2.57281E-05	8	2.58661E-05	6	2.58967E-05
7	2.57944E-05	3	2.58759E-05	5	2.59481E-05
8	2.58161E-05	5	2.60181E-05	8	2.59561E-05

40 FT*LBS		50 FT*LBS	
TRIAL	FINISH (s)	TRIAL	FINISH (s)
1	2.51127E-05	1	2.52127E-05
2	2.57327E-05	2	2.58827E-05
3	2.58959E-05	3	2.60259E-05
7	2.59344E-05	7	2.60544E-05
4	2.59893E-05	5	2.60781E-05
6	2.59967E-05	4	2.60893E-05
5	2.60181E-05	8	2.61261E-05
8	2.60661E-05	6	2.61267E-05

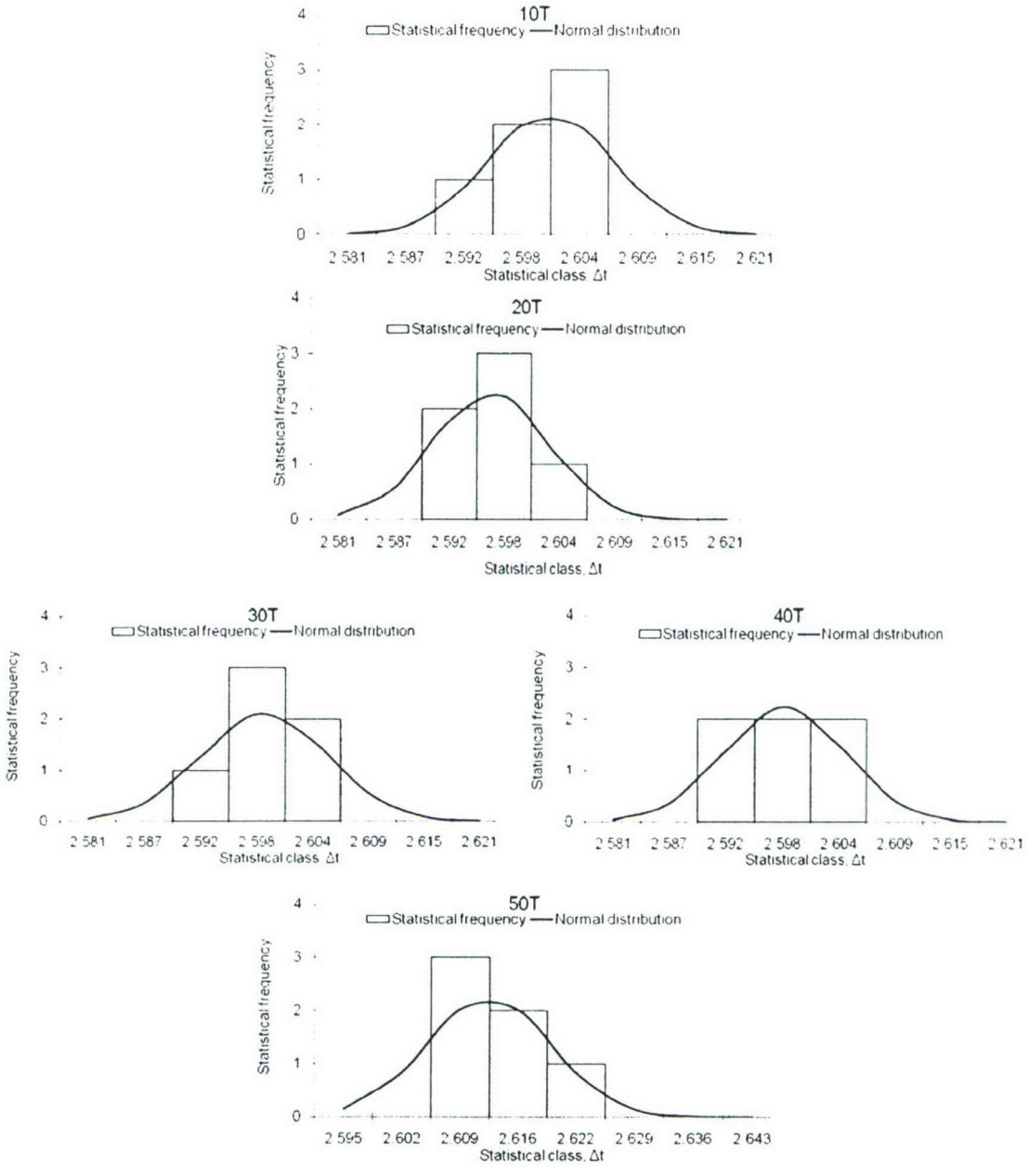

Figure 29 Experimentally determined statistical frequency and theoretically calculated normal distribution for statistical classes of torque settings 10 – 50 ft*lbs.

11 APPENDIX B
INVENTIONS

We submitted an invention disclosure entitled "A METHOD FOR ASSESSMENT OF BOLTED JOINT INTEGRITY USING NONLINEAR GUIDED WAVES" to New Mexico Tech administrative office.

Authors of the disclosure are: Andrei N. Zagrai and Derek T. Doyle.

12 APPENDIX C
PUBLICATIONS STEMMING FROM THE PROJECT

1. DOYLE, D., ZAGRAI, A. and ARRITT, B., (2007) "Elastic Waves for Structural Health Monitoring of Satellite Bolted Joints," A poster at *19th Annual Rio Grande Symposium on Advanced Materials*, 9 October 2007, The University of New Mexico, Albuquerque, NM.
2. ZAGRAI, A., DOYLE, D., and ARRITT, B., (2008) "Embedded Nonlinear Ultrasonics for Structural Health Monitoring of Satellite Joints," To appear in Proceedings of *SPIE's 15th Annual International Symposium on Smart Structures and Materials and 13th Annual International Symposium on NDE for Health Monitoring and Diagnostics*, 9-13 March 2008, San Diego, CA.
3. ARRITT, B.J., ROBERTSON, L.M., OUYANG, L., BEARD, S., CLAYTON, E., TODD, M.D., DOYLE, D., ZAGRAI, A., BUCKLEY, S.J., GANLEY, J.M., WELSH, J.S., (2008) "Structural Health Monitoring; an Enabler for Responsive Satellites," To appear in Proceedings of *SPIE's 15th Annual International Symposium on Smart Structures and Materials and 13th Annual International Symposium on NDE for Health Monitoring and Diagnostics*, 9-13 March 2008, San Diego, CA.
4. DOYLE, D., ARRITT, B., and ZAGRAI, A., (2008) "Potential Structural Health Monitoring Venues for Responsive Space Satellites," To appear in Proceedings of *49th AIAA/ASME/ASCE/AHS/ASC Structures, Structural Dynamics, and Materials Conference,* 7-10 April 2008, Chicago, Illinois, USA.

13 APPENDIX C
LIST OF PEOPLE INVOLVED IN RESEARCH EFFORTS

Derek Doyle – MS student

Daniel Kitts – MS student temporarily

Jerome Limoge – Undergraduate student

Emrah Kulunk – Undergraduate summer student

Alexey Belyaev – Summer researcher for 2 months.